INTERNATIONAL JOURNAL OF
NUMERICAL ANALYSIS AND MODELING
Volume 16, Number 3, Pages 436–462

OPTIMAL ERROR ESTIMATES OF THE LOCAL DISCONTINUOUS GALERKIN METHOD FOR THE TWO-DIMENSIONAL SINE-GORDON EQUATION ON CARTESIAN GRIDS

MAHBOUB BACCOUCH

Abstract. The sine-Gordon equation is one of the basic equations in modern nonlinear wave theory. It has applications in many areas of physics and mathematics. In this paper, we develop and analyze an energy-conserving local discontinuous Galerkin (LDG) method for the two-dimensional sine-Gordon nonlinear hyperbolic equation on Cartesian grids. We prove the energy conserving property, the L^2 stability, and optimal L^2 error estimates for the semi-discrete method. More precisely, we identify special numerical fluxes and a suitable projection of the initial conditions for the LDG scheme to achieve $p+1$ order of convergence for both the potential and its gradient in the L^2-norm, when tensor product polynomials of degree at most p are used. We present several numerical examples to validate the theoretical results. Our numerical examples show the sharpness of the $\mathcal{O}(h^{p+1})$ estimate.

Key words. Sine-Gordon equation, local discontinuous Galerkin method, energy conservation, L^2 stability, *a priori* error estimates, Cartesian grids.

1. Introduction

Developing energy-conserving and highly accurate numerical schemes to solve nonlinear hyperbolic partial differential equations (PDEs) is a very challenging scientific problem and is of fundamental importance to the simulation of waves and solitons. They are also important when dealing with coarse grids and large time steps. In this paper, we propose an energy-conserving local discontinuous Galerkin (LDG) method for the following two-dimensional sine-Gordon nonlinear hyperbolic equation

$$u_{tt} + \beta u_t + \sin(u) = \Delta u + f(x,y,t), \quad (x,y) \in \Omega = [a,b] \times [c,d], \ t \in [0,T], \tag{1a}$$

subject to the following initial conditions

$$u(x,y,0) = u_0(x,y), \quad u_t(x,y,0) = v_0(x,y), \quad (x,y) \in \Omega, \tag{1b}$$

and to either periodic boundary conditions

$$\begin{aligned} u(x,c,t) &= u(x,d,t), \quad u_y(x,c,t) = u_y(x,d,t), \\ u(a,y,t) &= u(b,y,t), \quad u_x(a,y,t) = u_x(b,y,t), \end{aligned} \tag{1c}$$

or mixed Dirichlet-Neumann boundary conditions

$$u = g_D, \quad (x,y) \in \partial\Omega_D \quad \text{and} \quad \nabla u \cdot \mathbf{n} = \mathbf{g}_N \cdot \mathbf{n}, \quad (x,y) \in \partial\Omega_N, \tag{1d}$$

for some given functions f, g, h, g_D, and $\mathbf{g}_N$. Here, $\partial\Omega = \partial\Omega_D \cup \partial\Omega_N$ is the boundary of the domain Ω, $\mathbf{n}$ is the outward unit normal to $\partial\Omega$, and $[0,T]$ is a finite time interval. The initial conditions $u_0(x,y)$ and $v_0(x,y)$ are the wave modes or kinks and velocity functions, respectively. In our theoretical analysis we select the initial/boundary conditions and the source, $f(x,y,t)$, such that the exact solution

Received by the editors September 13, 2017 and, in revised form, September 4, 2018.
2010 *Mathematics Subject Classification.* 65M12, 65M15, 65M60, 65N12, 65N30, 35Q51.

u is a smooth function on $\Omega \times [0, T]$. Our results may be extended to 3-D Cartesian meshes in straight forward manner. Details are not included to save space.

The nonlinear sine-Gordon equation plays an important role in modern physics; see *e.g.*, [44]. It is well-known that the sine-Gordon equation has soliton solutions in the one- and two-dimensional cases. The simplest of these solutions are called kinks and anti-kinks. It arises in many applications in physics, see *e.g.*, [25, 43, 53, 57, 61, 62]. For instance, the sine-Gordon equation arises in many different applications including propagation of magnetic flux on Josephson junctions, sound propagation in a crystal lattice, differential geometry, self-induced transparency, stability of fluid motion, laser physics, and particle physics. The two-dimensional equation (1a) arises in extended rectangular Josephson junctions, which consist of two layers of super conducting materials separated by an isolating barrier. The nonlinear term $\sin(u)$ is the Josephson current across an insulator between two superconductors [29]. Several other physical applications can be found in the review article by Barone *et al.* [25]. It is known (see *e.g.*, [64]) that the two-dimensional sine-Gordon equation (1a) with $\beta = f = 0$ and compactly supported or periodic boundary conditions admits the following important conserved quantity, called the total energy,

$$\begin{aligned} E(t) &= \frac{1}{2} \iint_{\Omega} \left(u_t^2 + u_x^2 + u_y^2 + 2(1 - \cos(u)) \right) dxdy \\ &= E_k(t) + E_s(t) + E_p(t), \end{aligned} \tag{2}$$

where the kinetic, strain, and potential energies are, respectively, defined by

$$E_k(t) = \frac{1}{2} \iint_{\Omega} u_t^2 dxdy, \quad E_s(t) = \frac{1}{2} \iint_{\Omega} (u_x^2 + u_y^2) dxdy,$$

$$E_p(t) = \iint_{\Omega} (1 - \cos(u)) dxdy.$$

Several numerical schemes have been developed in the literature for the sine-Gordon equation [1, 2, 26, 27, 35, 39, 40, 42, 46, 47, 48, 50, 51, 52, 55, 58, 59, 63, 67, 68, 71]. Among these methods, the finite-difference method, the finite-element method, the pseudospectral technique, the domain decomposition method. Some of these schemes are known to be energy-conserving. For instance, some energy-conserving second-order finite difference schemes have been proposed in [27, 41, 49, 66] and the references therein. These schemes are designed by using central second differences to approximate the second derivative terms in the PDE. The difference among the finite difference schemes is in the discretization of the nonlinear term $\sin(u)$. However, to the best of the author's knowledge, the application of the LDG method to (1a) has not been considered in the literature.

The main motivation for the LDG method proposed in this paper originates from the LDG techniques which have been successfully applied to many PDEs arising from a wide range of applications. The LDG finite element method is an extension of the discontinuous Galerkin (DG) method aimed at solving PDEs containing higher than first-order spatial derivatives. It was first introduced by Cockburn and Shu [38] for solving convection-diffusion problems. Since then, several LDG schemes have been developed and analyzed for various higher-order ordinary and partial differential equations in one and multiple dimensions including nonlinear two-point boundary-value problems [20], convection-diffusion problems [3, 7, 10, 16, 24], second-order wave equations [6, 12, 13, 14, 17], the sine-Gordon

equation [18, 19, 21, 22], KdV-type equations [15, 23], and the fourth-order Euler-Bernoulli beam equation [8, 9, 11], just to mention a few. DG methods are suitable numerical schemes for solving a wide class of engineering problems. Robustness, local conservation, and flexibility for implementing *hp*-adaptivity strategies are well-known advantages of DG methods stemming from the use of finite element spaces consisting of discontinuous piecewise polynomials. They can be locally conservative and capable of dealing naturally with discontinuous physical properties. The DG method was initially proposed by Reed and Hill in 1973 as a technique to solve neutron transport problems [60]. Lesaint and Raviart [54] provided the first numerical analysis of the DG method for the linear advection equation. Since then, DG methods have been used to solve many PDEs including hyperbolic, elliptic, and parabolic equations. Consult [37, 65] and the references cited therein for a detailed discussion of the history of DG methods and a list of important citations on their applications to science and engineering.

The LDG method shares the advantages of the standard DG methods, such as good stability, high order accuracy, and flexibility to handle complex geometry. One of the advantages of the proposed method over the existing numerical schemes in the literature is that the proposed LDG scheme achieves optimal $(p+1)$th order convergence for the solution and its gradient in the L^2-norm. Furthermore, this LDG method achieves superconvergence results which can be used to construct asymptotically exact *a posteriori* error estimates by solving a local steady problem on each element; see [19]. There are many other motivations for using LDG methods. For instance, stability is provided without slope limiters by carefully choosing the numerical fluxes, they can achieve high order accuracy for smooth functions while being non-oscillatory near discontinuities, and they are element-wise conservative. This last property is very useful in the area of computational fluid dynamics, especially in situations where there are shocks, steep gradients or boundary layers. Moreover, LDG methods are extremely flexible in the mesh-design; they can easily handle meshes with hanging nodes, elements of various types and shapes, and local spaces of different orders. They further achieve global superconvergence that can be used to estimate the global discretization errors. We also mention that our proposed semi-discrete scheme is shown to be energy-conserving for the physical energy. The energy-conserving property is one of the guiding principles for numerical algorithms because it provides an accurate approximation and minimizes the phase or shape errors after long time integration. Finally, the LDG method can also be designed for many other higher-order nonlinear wave and diffusion equations. Examples include the KdV equations, the Kadomtsev-Petviashvili equations, the Zakharov-Kuznetsov equations, the Kuramoto-Sivashinsky-type equations, the Cahn-Hilliard equation, and the equations for surface diffusion and Willmore flow of graphs. Consult [69] for more details.

It is well-known that energy-conserving schemes for wave propagation problems are very suitable for long time simulations. In [18], we proposed and analyzed a high-order and energy-conserving LDG method for the sine-Gordon nonlinear hyperbolic equation in one space dimension. We proved the energy-conserving property, the L^2 stability, and optimal *a priori* error estimates for the solution and for the auxiliary variable that approximates the first-order derivative. The order of convergence is proved to be $p+1$, when piecewise polynomials of degree at most p are used. Our numerical experiments demonstrate optimal order of convergence. In [19], we investigated the superconvergence properties of the LDG method applied to the

two-dimensional sine-Gordon nonlinear hyperbolic equation on Cartesian grids. We performed a local error analysis and showed that the actual error can be split into an $\mathcal{O}(h^{p+1})$ leading component and a high order component, when tensor product polynomials of degree at most p are used. We further proved that the leading term of the LDG error is spanned by two $(p+1)$-degree Radau polynomials in the x and y directions, respectively. Thus, the LDG solution is $\mathcal{O}(h^{p+2})$ superconvergent at Radau points obtained as a tensor product of the roots of $(p+1)$-degree right Radau polynomials. Computational results suggest that these superconvergence results hold globally, but it remains an open problem to investigate the global superconvergence results. We used these results to construct simple, efficient, and asymptotically exact *a posteriori* LDG error estimates. These estimates are computationally simple and are obtained by solving local steady problems with no boundary conditions on each element. We would like to emphasize that these results are based on local error analysis and there is no theoretical justification of these results so far. This paper is a natural continuation of the work done in [19]. We prove optimal error estimates and the energy-conserving property for the semi-discrete LDG method.

In this paper, we present a high order and energy-conserving LDG method for the two-dimensional sine-Gordon equation on Cartesian grids. We prove that the semi-discrete LDG formulation conserves a discrete version of the continuous energy for all time. The L^2 stability of the semi-discrete LDG method is also proved. We further identify special numerical fluxes and a suitable projection of the initial conditions for the LDG scheme to prove optimal L^2 error estimates for the semi-discrete formulation. The L^2 errors for the potential and its gradient are shown to converge with the optimal order $\mathcal{O}(h^{p+1})$, when tensor product polynomials of degree at most p are used. We would like to mention that the proposed LDG method has considerable advantages over the numerical method available in the literature. The main advantages include: (i) it conserves the discrete approximation of energy and consequently it can maintain the phase and shape of the waves accurately, especially for long time simulation, (ii) it achieves stability without slope limiters, (iii) it exhibits optimal convergence properties for the solution and for the auxiliary variables that approximate the first-order partial derivatives, (iv) it is extremely flexible in the mesh-design (it can easily handle meshes with hanging nodes, elements of various types and shapes, and local spaces of different orders), and (v) it achieves superconvergence results which can be used to construct asymptotically exact *a posteriori* error estimates by solving a local steady problem on each element; see [19].

The rest of the paper is organized as follows: In section 2, we present the LDG method for solving (1) and we introduce some preliminary results. We prove the energy conservation and L^2 stability of the LDG scheme in section 3. In section 4, we present the LDG error analysis and prove optimal L^2 error estimates for the semi-discrete LDG method. In section 5, we present several numerical results to validate our theoretical results. Concluding remarks are given in section 6.

2. The LDG method and preliminary results

2.1. The semi-discrete LDG method for the sine-Gordon equation. To define the semi-discrete LDG method, we introduce an auxiliary variable $\mathbf{q} = \nabla u$ and rewrite our model equation (1a) as a first-order system in space:

$$u_{tt} + \beta u_t + \sin(u) - \nabla \cdot \mathbf{q} = f, \qquad \mathbf{q} - \nabla u = 0. \tag{3}$$

Next, we discretize (3) in space by using the LDG method, while leaving time continuous. We divide the computational domain $\Omega = [a, b] \times [c, d]$ into a Cartesian grid $\mathcal{T}_h$ consisting of $N = n \times m$ shape-regular rectangle elements $\Delta_{ij} = [x_{i-1}, x_i] \times [y_{j-1}, y_j] = I_i \times J_j$, $i = 1, 2, \ldots, n$, $j = 1, 2, \ldots, m$, where $a = x_0 < x_1 < \cdots < x_n = b$ and $c = y_0 < y_1 < \cdots < y_m = d$. We denote the lengths of the intervals $I_i = [x_{i-1}, x_i]$ and $J_j = [y_{j-1}, y_j]$ by $\Delta x_i = x_i - x_{i-1}$ and $\Delta y_j = y_j - y_{j-1}$, respectively. We also use $h = \max\limits_{1\le i\le n,\ 1\le j\le m}(\Delta x_i, \Delta y_j)$ and $h_{min} = \min\limits_{1\le i\le n,\ 1\le j\le m}(\Delta x_i, \Delta y_j)$ to denote the length of the largest and smallest mesh size, respectively. We shall consider regular meshes in the sense that $h \le K h_{min}$, where $K \ge 1$ is a constant (independent of h) during mesh refinement. If $K = 1$, then the mesh is uniformly distributed. In the remainder of this paper, we omit the element index and refer to an arbitrary element by Δ whenever confusion is unlikely.

Multiplying the two equations in (3) by arbitrary smooth test functions v and $\mathbf{w}$, integrating over an arbitrary element Δ, and applying Green's theorem, we obtain

$$\text{(4a)} \qquad \iint_\Delta \left(u_{tt} + \beta u_t + \sin(u)\right) v dxdy + \iint_\Delta \mathbf{q} \cdot \nabla v dxdy - \int_\Gamma v\mathbf{q} \cdot \mathbf{n} ds$$
$$= \iint_\Delta f v dxdy,$$
$$\text{(4b)} \qquad \iint_\Delta \mathbf{q} \cdot \mathbf{w}\ dxdy + \iint_\Delta u \nabla \cdot \mathbf{w} dxdy - \int_\Gamma u\ \mathbf{w} \cdot \mathbf{n}\ ds = 0,$$

where Γ is the boundary of the element Δ and $\mathbf{n}$ is the unit outward normal vector to Γ.

Let $\mathcal{Q}^p(\Delta)$ be the tensor product space consisting of polynomials on the element Δ with coefficients as functions of t, where the degree in each variable does not exceed p. We also define the global discontinuous finite element spaces V_h^p and $\mathbf{V}_h^p$ as

$$V_h^p = \{u \in L^2(\Omega) :\ u|_\Delta \in \mathcal{Q}^p(\Delta),\ \forall\ \Delta \in \mathcal{T}_h\},$$
$$\mathbf{V}_h^p = \{\mathbf{q} \in [L^2(\Omega)]^2\ :\ \mathbf{q}|_\Delta \in [\mathcal{Q}^p(\Delta)]^2,\ \forall\ \Delta \in \mathcal{T}_h\}.$$

Note that polynomials in the spaces V_h^p and $\mathbf{V}_h^p$ are allowed to have discontinuities across element boundaries.

For a given partition $\mathcal{T}_h$ of Ω, we approximate the exact solutions u and $\mathbf{q}$ at fixed time t by piecewise polynomials $u_h \in V_h^p$ and $\mathbf{q}_h \in \mathbf{V}_h^p$. We note that u_h and $\mathbf{q}_h$ are piecewise polynomials not necessarily continuous across inter-element boundaries. Thus, we consider the following semi-discrete LDG method: find $u_h \in V_h^p$ and $\mathbf{q}_h \in \mathbf{V}_h^p$ such that

$$\text{(5a)} \qquad \iint_\Delta \left((u_h)_{tt} + \beta (u_h)_t + \sin(u_h)\right) v dxdy + \iint_\Delta \mathbf{q}_h \cdot \nabla v dxdy - \int_\Gamma v \hat{\mathbf{q}}_h \cdot \mathbf{n} ds$$
$$= \iint_\Delta f v dxdy,$$
$$\text{(5b)} \qquad \iint_\Delta \mathbf{q}_h \cdot \mathbf{w} dxdy + \iint_\Delta u_h \nabla \cdot \mathbf{w}\ dxdy - \int_\Gamma \hat{u}_h\ \mathbf{w} \cdot \mathbf{n} ds = 0,$$

for all test functions $v \in V_h^p$, $\mathbf{w} \in \mathbf{V}_h^p$, and for all $\Delta \in \mathcal{T}_h$. Here, the functions $\hat{u}_h$ and $\hat{\mathbf{q}}_h$ are the so-called *numerical fluxes* which are nothing but discrete approximations to the traces of u and $\mathbf{q}$ on the boundary Γ.

The initial conditions $u_h(x,y,0) \in V_h^p$ and $(u_h)_t(x,y,0) \in V_h^p$ are obtained using a special projection of the exact initial conditions $u(x,y,0)$ and $u_t(x,y,0)$, respectively. This particular projection will be defined later.

To complete the definition of the semi-discrete LDG method we need to select $\hat{u}_h$ and $\hat{\mathbf{q}}_h$ on the boundaries of Δ. We would like to mention that the choice of the numerical fluxes is perhaps the most delicate and crucial aspect of the definition of the LDG methods as it can affect their consistency, stability, and even accuracy. To define these numerical fluxes, we need to introduce some notation. For simplicity, we use $v^-(x_i,\cdot,\cdot)$ and $v^+(x_i,\cdot,\cdot)$ to denote the left limit and the right limit of v at the discontinuity point (x_i, y) and time t, *i.e.*,

$$v^-(x_i,y,t) = v(x_i^-,y,t) = \lim_{s\to 0^-} v(x_i+s,y,t),$$

$$v^+(x_i,y,t) = v(x_i^+,y,t) = \lim_{s\to 0^+} v(x_i+s,y,t).$$

Similarly, we use $v^-(x,y_j,t) = v(x,y_j^-,t)$ and $v^+(x,y_j,t) = v(x,y_j^+,t)$.

Based on the LDG method for elliptic problems introduced by Cockburn *et al.* [36, 38], we first use an arbitrary but fixed vector $\mathbf{v}$ with nonzero components to define artificial outflow and inflow boundaries. The role of the vector $\mathbf{v}$ is to give a single rule to pick the numerical fluxes $\hat{u}_h$ and $\hat{\mathbf{q}}_h$ for all the elements. For simplicity, we choose $\mathbf{v} = [1,1]^t$ and we define artificial inflow and outflow boundaries

$$\partial\Omega^+ = \{(x,y) \in \partial\Omega \mid \mathbf{v}\cdot\mathbf{n} \geq 0\} = \partial\Omega_1^+ \cup \partial\Omega_2^+, \quad \partial\Omega^- = \partial\Omega\backslash\partial\Omega^+ = \partial\Omega_1^- \cup \partial\Omega_2^-,$$

where $\partial\Omega_1^-$, $\partial\Omega_1^+$, $\partial\Omega_2^-$, and $\partial\Omega_2^+$ denote the left, right, bottom, and top edges of the domain Ω, respectively.

We also define the boundary of each element $\Delta \in \mathcal{T}_h$ as $\Gamma = \Gamma^- \cup \Gamma^+$, where the artificial inflow Γ^- and outflow Γ^+ boundaries are defined by

$$\Gamma^+ = \{(x,y) \in \Gamma \mid \mathbf{v}\cdot\mathbf{n} \geq 0\} = \Gamma_1^+ \cup \Gamma_2^+, \quad \Gamma^- = \Gamma\backslash\Gamma^+ = \Gamma_1^- \cup \Gamma_2^-,$$

and Γ_1^-, Γ_1^+, Γ_2^-, and Γ_2^+ are used to denote the left, right, bottom, and top edges of the element Δ, respectively.

Now, we are ready to define the numerical fluxes. For the periodic boundary conditions, we choose the following alternating fluxes

$$\hat{u}_h = u_h^-, \quad \hat{\mathbf{q}}_h = \mathbf{q}_h^+. \tag{5c}$$

That is, if Γ is any edge, then, on the vertical edges, $\hat{u}_h$ is always equal to trace of u from the left, and on horizontal edges, $\hat{u}_h$ is always equal to the trace of u from below. Similarly, $\hat{\mathbf{q}}_h$ is the right trace of $\mathbf{q}$ on the vertical edges and the trace of $\mathbf{q}$ from above on the horizontal edges. As discussed in [13], this particular choice is not unique. In fact the choice $\hat{u}_h = u_h^+$ and $\hat{\mathbf{q}}_h = \mathbf{q}_h^-$ yields similar results.

For the Dirichlet and mixed boundary conditions (1d), we use the so-called the minimal dissipation LDG (md-LDG) method; see, *e.g.*, [6, 7, 8, 10, 14, 30, 31, 56]. More precisely, on interior edges, we can still take the alternating fluxes

$$\hat{u}_h = u_h^-, \quad \hat{\mathbf{q}}_h = \mathbf{q}_h^+. \tag{5d}$$

However, if Γ lies on the boundary of Ω, we take

$$\text{(5e)} \qquad \hat{u}_h = \begin{cases} P^- g_D, \ (x,y) \in \partial\Omega_D, \\ u_h^-, \ (x,y) \in \partial\Omega_N \cap \partial\Omega^+, \\ u_h^+, \ (x,y) \in \partial\Omega_N \cap \partial\Omega^-, \end{cases}$$

$$\hat{\mathbf{q}}_h = \begin{cases} \mathbf{g}_N, \ (x,y) \in \partial\Omega_N, \\ \mathbf{q}_h^+, \ (x,y) \in \partial\Omega_D \cap \partial\Omega^-, \\ \mathbf{q}_h^- - c_{11}(u_h^- - P^- g_D)\ \mathbf{n}, \ (x,y) \in \Gamma_b \subset \partial\Omega_D \cap \partial\Omega^+, \end{cases}$$

where c_{11} is the stabilization parameter for our LDG method and P^- is the Gauss-Radau projection defined in (8). The stabilization parameter is defined as follows: if h is the length of an edge $\Gamma \subset \partial\Omega^+$, then $c_{11} = p/h_{\Gamma_b}$; otherwise $c_{11} = 0$, where h_{Γ_b} is the length of the edge Γ_b.

Remark 2.1. *We would like to emphasize that this two-dimensional md-LDG method applies stabilization only on the artificial outflow boundary. The distinctive feature of the md-LDG method is that the stabilization parameter associated with the numerical trace of* $\mathbf{q}$ *is taken to be identically zero on all interior nodes. In other words, only the numerical flux on the boundary* $\partial\Omega_D \cap \partial\Omega^+$ *is penalized and this is why its dissipation is said to be minimal. In* [3, 13, 19]*, we applied the same numerical fluxes to investigate the superconvergence properties of the md-LDG method for two-dimensional elliptic, parabolic, and hyperbolic equations on Cartesian meshes.*

Remark 2.2. *We remark that the auxiliary nonzero vector* $\mathbf{v}$ *is an arbitrary but fixed vector. It is used to define the artificial outflow and inflow boundaries. Thus, if other vector* $\mathbf{v}$ *is chosen, the artificial outflow and inflow boundaries* $\partial\Omega^{\pm}$ *must be changed accordingly.*

2.2. Notation and definitions. We denote by $\mathcal{E}_B$ the set of all boundary edges of the triangulation $\mathcal{T}_h$ on $\partial\Omega$ and by $\mathcal{E}_I$ the set of all interior edges of the triangulation $\mathcal{T}_h$. We use $\mathcal{E}$ to denote all edges *i.e.*, $\mathcal{E} = \mathcal{E}_B \cup \mathcal{E}_I$. We also use $\mathcal{E}_D$ and $\mathcal{E}_N$ to denote the set of edges on $\partial\Omega_D$ and $\partial\Omega_N$, respectively.

In this paper, we define the L^2 inner product of two integrable functions, u and v, on $\Delta \in \mathcal{T}_h$ as

$$(u,v)_\Delta = \iint_\Delta u(x,y,t)v(x,y,t)dxdy.$$

Denote $\|u\|_{0,\Delta}^2 = (u,u)_\Delta$ to be the standard L^2-norm of u on Δ. Let $H^s(\Delta)$, where $s = 1, 2, \ldots$, denote the standard Sobolev space. For any real-valued function u in $H^s(\Delta)$, the $H^s(\Delta)$-norm over Δ is

$$\|u\|_{s,\Delta} = \left(\sum_{|\alpha| \le s} \|D^\alpha u\|_\Delta^2 \right)^{1/2}.$$

For any vector-valued function $\mathbf{q} = [q_1, q_2]^t \in \mathbf{H}^s(\Delta) = [H^s(\Delta)]^2$, the $\mathbf{H}^s(\Delta)$-norm over Δ is

$$\|\mathbf{q}\|_{s,\Delta} = \left(\sum_{i=1}^{2} \|q_i\|_{s,\Delta}^2 \right)^{1/2}.$$

We also define the norms on the whole computational domain Ω as follows:

$$\|u\|_{s,\Omega} = \left(\sum_{\Delta \in \mathcal{T}_h} \|u\|_{s,\Delta}^2 \right)^{1/2}, \qquad \|\mathbf{q}\|_{s,\Omega} = \left(\sum_{\Delta \in \mathcal{T}_h} \|\mathbf{q}\|_{s,\Delta}^2 \right)^{1/2}.$$

For simplicity, we use $\|u\|$ and $\|u\|_s$ to denote $\|u\|_{0,\Omega}$ and $\|u\|_{s,\Omega}$, respectively. We also use $\|u(t)\|$ to denote the value of $\|u(\cdot,\cdot,t)\|$ at time t. In particular, we use $\|u(0)\|$ to denote $\|u(\cdot,\cdot,0)\|$. Throughout the paper, we omit the argument t and we use $\|u\|$ to denote $\|u(t)\|$ whenever confusion is unlikely.

2.3. Projections. We first introduce some one-dimensional projections. Let $I_i = [x_{i-1}, x_i]$ be any interval and let $\mathbb{P}^p(I_i)$ be the space of polynomials of degree not exceeding p on I_i. We denote by P_x the L^2-projection onto $\mathbb{P}^p(I_i)$, *i.e.*, for a function $u \in L^2(I_i)$ the projection $P_x u$ is the unique polynomial in $\mathbb{P}^p(I_i)$ satisfying

$$\int_{I_i} (P_x u - u) v dx = 0, \ \forall\ v \in \mathbb{P}^p(I_i). \tag{6}$$

Furthermore, we consider two one-dimensional Gauss-Radau projections, $P_x^{\pm}$, which are defined as follows: For a function u, the restriction of $P_x^- u$ to I_i is the unique polynomial in $\mathbb{P}^p(I_i)$ satisfying the $p+1$ conditions

$$\int_{I_i} (P_x^- u - u) v dx = 0, \ \forall\ v \in \mathbb{P}^{p-1}(I_i) \quad \text{and} \quad (P_x^- u)^- = u^- \quad \text{at } x = x_i. \tag{7a}$$

Similarly, the restriction of $P_x^+ u$ to I_i is the unique polynomial in $\mathbb{P}^p(I_i)$ satisfying

$$\int_{I_i} (P_x^+ u - u) v dx = 0, \ \forall\ v \in \mathbb{P}^{p-1}(I_i) \quad \text{and} \quad (P_x^+ u)^+ = u^+ \quad \text{at } x = x_{i-1}. \tag{7b}$$

Next, we introduce a two-dimensional Gauss-Radau projection. Let $\Delta = I_i \times J_j$, where $I_i = [x_{i-1}, x_i]$ and $J_j = [y_{j-1}, y_j]$, be an arbitrary rectangle element. The projection P^- for a scalar function u is defined as tensor product of the projections in one dimension (see *e.g.*, [36])

$$P^- u = P_x^- \otimes P_y^- u, \tag{8}$$

with $\otimes$ denoting the standard tensor product, with the subscripts x and y indicating the application of the one-dimensional operator, defined in (7), with respect to the corresponding variable. We note that the projection P^- on the Cartesian meshes has the following superconvergence property [36].

Lemma 2.1. *Let $Z_\Delta(u, \mathbf{w})$ be defined by*

$$Z_\Delta(u, \mathbf{w}) = \iint_\Delta (u - P^- u) \nabla \cdot \mathbf{w} dx dy - \int_\Gamma (u - P^- u)^- \mathbf{w} \cdot \mathbf{n} ds. \tag{9}$$

If $u \in H^{p+2}(\Omega)$ and $\mathbf{w} \in \mathbf{V}_h^p$ then

$$\sum_{\Delta \in \mathcal{T}_h} \left| Z_\Delta(u, \mathbf{w}) \right| \le C h^{p+1} \|u\|_{p+2} \|\mathbf{w}\|, \tag{10}$$

where C depends solely on p and the shape-regular constant.

Proof. The proof is given in [36], more precisely in its Lemma 3.6. □

Finally, we define a projection $\mathbf{P}^+$ for vector-valued function $\mathbf{q} = [q_1, q_2]^t$ as follows [36]

$$\mathbf{P}^+ \mathbf{q} = [P_x^+ \otimes P_y q_1, P_x \otimes P_y^+ q_2]^t, \tag{11}$$

where P_x and P_y are the standard L^2-projections in the x-direction and y-direction, respectively. One can easily show that, for any smooth vector-valued function $\mathbf{q}$, the restriction of $\mathbf{P}^+ \mathbf{q}$ to Δ is the element of $[\mathcal{Q}^p(\Delta)]^2$ satisfying

$$\iint_\Delta (\mathbf{P}^+ \mathbf{q} - \mathbf{q}) \cdot \nabla v dx dy = 0 \quad \text{and} \quad \int_{\Gamma^-} (\mathbf{P}^+ \mathbf{q} - \mathbf{q})^+ \cdot \mathbf{n} v^+ ds = 0, \quad \forall\ v \in \mathcal{Q}^p(\Delta). \tag{12}$$

It can be easily seen that the conditions in (12) uniquely define the projection $\mathbf{P}^+\mathbf{q}$.

We would like to mention that the above special projections are used in the error estimates of the LDG methods to derive optimal L^2 error bounds in the literature, *e.g.*, in [36].

In our analysis, we need several approximation results. Their proofs can be found in [36, 45, 70].

Lemma 2.2. *For any $u \in H^{p+1}(\Omega)$ and $\mathbf{q} \in [H^{p+1}(\Omega)]^2$, there exists a constant C independent of h such that*

$$\left\|u - P^- u\right\| \leq Ch^{p+1} \left\|u\right\|_{p+1}, \qquad \left\|\mathbf{q} - \mathbf{P}^+\mathbf{q}\right\| \leq Ch^{p+1} \left\|\mathbf{q}\right\|_{p+1}. \tag{13}$$

2.4. Initial conditions for the LDG scheme. To obtain optimal error estimates, we carefully design suitable projections of the initial conditions for the LDG scheme. In our mathematical error analysis and numerical examples, we approximate the initial conditions of our LDG scheme on each interval as follows

$$u_h(x,y,0) = P^- u(x,y,0), \quad (u_h)_t(x,y,0) = P^- u_t(x,y,0), \quad (x,y) \in \Delta, \quad \forall\, \Delta \in \mathcal{T}_h. \tag{14}$$

These approximated initial conditions are needed for technical purposes in the proof of the error estimates.

Remark 2.3. *We would like to emphasize that the special choice of the approximated initial conditions is necessary in the prove of optimal convergence rates of the proposed LDG scheme. In our numerical experiments, we used the standard L^2-projections for both $u(x,y,0)$ and $u_t(x,y,0)$ to approximate the initial conditions of our numerical scheme and observed that the convergence rate does not converge to the desired $p+1$ accuracy. Our special projection P^- is designed to better control the error of the initial conditions and it has an impact on the convergence results (see section 4).*

3. Energy conservation and L^2 stability of the semi-discrete LDG scheme

3.1. Energy conservation of the semi-discrete LDG scheme. The conservation of the energy for sine-Gordon equations is an important characteristic of the nonlinear solitary waves. Also schemes conserving the discrete analogs of energy often produce approximations that behave better for long time simulation.

Next, we will show that the proposed semi-discrete LDG method conserves the following discrete energy

$$E_h(t) = \frac{1}{2} \iint_{\Omega} \left(((u_h)_t)^2 + q_{1,h}^2 + q_{2,h}^2 + 2(1 - \cos(u_h)) \right) dxdy, \tag{15}$$

where $q_{1,h}$ and $q_{2,h}$ are the components of $\mathbf{q}_h$, *i.e.*, $\mathbf{q}_h = [q_{1,h}, q_{2,h}]^t$. We note that (15) is a consistent approximation of the continuous energy (2) since u_h, $q_{1,h}$ and $q_{2,h}$ are approximations to u, $q_1 = u_x$ and $q_2 = u_y$, respectively.

Theorem 3.1. *The discrete energy $E_h(t)$ defined in (15) is conserved by the semi-discrete LDG method (5) with $\beta = f = 0$ and compactly supported or periodic boundary conditions for all time i.e.,*

$$E_h(t) = E_h(0), \quad \forall\, t \in [0,T]. \tag{16a}$$

If $\beta > 0$ and $f = 0$, then $E_h(t)$ is dissipative for all time i.e.,

$$0 \leq E_h(t) \leq E_h(0), \quad \forall\, t \in [0,T]. \tag{16b}$$

Proof. Using the numerical fluxes defined in (5c) and a simple integration by parts, we write (5a) with $f = 0$ as

$$\begin{aligned} &\iint_{\Delta} \left((u_h)_{tt} + \beta(u_h)_t + \sin(u_h) - \nabla \cdot \mathbf{q}_h\right) v dxdy \\ &- \int_{\Gamma^+} v^- (\mathbf{q}_h^+ - \mathbf{q}_h^-) \cdot \mathbf{n} ds = 0. \end{aligned} \tag{17}$$

We choose $v = (u_h)_t$ in (17), then we take the first time derivative of (5b) and we choose $\mathbf{w} = \mathbf{q}_h$ to get

$$\iint_{\Delta} \left((u_h)_{tt} + \beta(u_h)_t + \sin(u_h) - \nabla \cdot \mathbf{q}_h\right) (u_h)_t dxdy$$

$$- \int_{\Gamma^+} (u_h)_t^- (\mathbf{q}_h^+ - \mathbf{q}_h^-) \cdot \mathbf{n} ds = 0, \tag{18a}$$

$$\iint_{\Delta} (\mathbf{q}_h)_t \cdot \mathbf{q}_h dxdy + \iint_{\Delta} (u_h)_t \nabla \cdot \mathbf{q}_h dxdy - \int_{\Gamma} (u_h)_t^- \mathbf{q}_h \cdot \mathbf{n} ds = 0. \tag{18b}$$

Adding the two equations in (18), we get

$$\begin{aligned} \iint_{\Delta} (\mathbf{q}_h)_t \cdot \mathbf{q}_h dxdy + \iint_{\Delta} \left((u_h)_{tt} + \beta(u_h)_t + \sin(u_h)\right) (u_h)_t dxdy = \\ \int_{\Gamma^+} (u_h)_t^- \mathbf{q}_h^+ \cdot \mathbf{n} ds + \int_{\Gamma^-} (u_h)_t^- \mathbf{q}_h^+ \cdot \mathbf{n} ds. \end{aligned}$$

Summing over all elements and noticing that the sum on the right-hand side telescopes yields

$$\begin{aligned} &\frac{1}{2}\frac{d}{dt} \iint_{\Omega} \left(\mathbf{q}_h \cdot \mathbf{q}_h + (u_h)_t^2 + 2\left(1 - \cos(u_h)\right)\right) dxdy \\ &= \int_{\mathcal{E}_B} (u_h)_t^- \mathbf{q}_h^+ \cdot \mathbf{n} ds - \beta \iint_{\Omega} (u_h)_t^2 dxdy. \end{aligned} \tag{19}$$

For the periodic or compactly supported boundary conditions, the integral over $\mathcal{E}_B$ vanishes and (19) becomes

$$\frac{1}{2}\frac{d}{dt} \iint_{\Omega} \left(\mathbf{q}_h \cdot \mathbf{q}_h + (u_h)_t^2 + 2\left(1 - \cos(u_h)\right)\right) dxdy = -\beta \iint_{\Omega} (u_h)_t^2 dxdy \leq 0,$$

since $\beta \geq 0$.

Integrating with respect to time from 0 to t, we establish (16). □

Remark 3.1. *Equation (16a) indicates that the semi-discrete LDG method conserves the discrete energy $E_h(t)$. The energy-conserving property is one of the guiding principles for numerical algorithms because it provides an accurate approximation and minimizes the phase or shape errors after long time integration.*

3.2. L^2 stability. Here, we will prove the following L^2 stability results for the LDG scheme (5).

Theorem 3.2. *Suppose $f = 0$. For periodic or compactly supported boundary conditions for the computation domain Ω, the numerical solution given by the LDG method defined by (5) satisfies the following L^2 stability*

$$\|(u_h)_t\|^2 + \|\mathbf{q}_h\|^2 \leq \|(u_h)_t(0)\|^2 + \|\mathbf{q}_h(0)\|^2 + \|u_h(0)\|^2. \tag{20a}$$

$$\begin{aligned} \|u_h\|^2 \leq &2(1 + T(1+\beta) + T^2) \|u_h(0)\|^2 + 2(T + T^2) \|(u_h)_t(0)\|^2 \\ &+ 2T^2 \|\mathbf{q}_h(0)\|^2 + T^4(b-a)(d-c). \end{aligned} \tag{20b}$$

Proof. Using (16) and the fact that $1-\cos(u_h)\geq 0$, we have

$$\begin{aligned}&\frac{1}{2}\left\|(u_h)_t\right\|^2+\frac{1}{2}\left\|\mathbf{q}_h\right\|^2\leq E_h(t)\leq E_h(0)\\ =&\frac{1}{2}\left\|(u_h)_t(0)\right\|^2+\frac{1}{2}\left\|\mathbf{q}_h(0)\right\|^2+\iint_{\Omega}\left(1-\cos(u_h(x,y,0))\right)dxdy.\end{aligned}\tag{21}$$

Using the classical Taylor's theorem with integral remainder in the variable u, we write

$$1-\cos(u_h(x,y,0))=\theta(x,y)\ u_h^2(x,y,0),\tag{22}$$

where θ is the mean value given by $\theta(x,y)=-\frac{1}{2}\int_0^1 s\cos(su_h(x,y,0))ds$. We note that

$$\left|\theta(x,y)\right|\leq\frac{1}{2}\int_0^1\left|s\cos(su_h(x,y,0))\right|ds\leq\frac{1}{2},\quad\forall\ (x,y)\in\Omega.\tag{23}$$

Using (22) and applying the estimate (23), (21) yields

$$\begin{aligned}\frac{1}{2}\left\|(u_h)_t\right\|^2+\frac{1}{2}\left\|\mathbf{q}_h\right\|^2\leq&\frac{1}{2}\left\|(u_h)_t(0)\right\|^2+\frac{1}{2}\left\|\mathbf{q}_h(0)\right\|^2+\iint_{\Omega}\theta(x,y)\ u_h^2(x,y,0)dxdy\\ \leq&\frac{1}{2}\left\|(u_h)_t(0)\right\|^2+\frac{1}{2}\left\|\mathbf{q}_h(0)\right\|^2+\frac{1}{2}\left\|u_h(0)\right\|^2,\end{aligned}$$

which completes the proof of (20a).

Next, we will prove (20b). Taking $v=u_h$ in (17) and $\mathbf{w}=\mathbf{q}_h$ in (5b) we obtain

$$\iint_{\Delta}\left((u_h)_{tt}+\beta(u_h)_t+\sin(u_h)-\nabla\cdot\mathbf{q}_h\right)u_h dxdy-\int_{\Gamma^+}u_h$$

$$-(\mathbf{q}_h^+-\mathbf{q}_h^-)\cdot\mathbf{n}ds=0,\tag{24a}$$

$$\iint_{\Delta}\mathbf{q}_h\cdot\mathbf{q}_h dxdy+\iint_{\Delta}u_h\nabla\cdot\mathbf{q}_h dxdy-\int_{\Gamma}u_h^-\mathbf{q}_h\cdot\mathbf{n}ds=0.\tag{24b}$$

Adding the two equations in (24), we obtain

$$\begin{aligned}&\iint_{\Delta}\left((u_h)_{tt}+\beta(u_h)_t+\sin(u_h)\right)u_h dxdy+\iint_{\Delta}\mathbf{q}_h\cdot\mathbf{q}_h dxdy\\ =&\int_{\Gamma^+}u_h^-\mathbf{q}_h^+\cdot\mathbf{n}ds+\int_{\Gamma^-}u_h^-\mathbf{q}_h^+\cdot\mathbf{n}ds.\end{aligned}\tag{25}$$

Summing (25) over all elements and applying the periodic or compactly supported boundary conditions yields

$$\iint_{\Omega}(u_h)_{tt}u_h dxdy+\beta\iint_{\Omega}(u_h)_t u_h dxdy+\iint_{\Omega}\sin(u_h)u_h dxdy+\iint_{\Omega}\mathbf{q}_h\cdot\mathbf{q}_h dxdy=0.\tag{26}$$

Using the relation $(u_h)_{tt}u_h=\left(u_h(u_h)_t\right)_t-((u_h)_t)^2=\frac{1}{2}\left(u_h^2\right)_{tt}-((u_h)_t)^2$, the estimate (20a), and the Cauchy-Schwarz inequality, we get

$$\begin{aligned}&\frac{1}{2}\frac{d^2\left\|u_h\right\|^2}{dt^2}+\frac{\beta}{2}\frac{d\left\|u_h\right\|^2}{dt}+\left\|\mathbf{q}_h\right\|^2\\ =&\left\|(u_h)_t\right\|^2-\iint_{\Omega}\sin(u_h)u_h dxdy\\ \leq&\left\|(u_h)_t(0)\right\|^2+\left\|\mathbf{q}_h(0)\right\|^2+\left\|u_h(0)\right\|^2+\iint_{\Omega}|u_h|dxdy\\ \leq&\left\|(u_h)_t(0)\right\|^2+\left\|\mathbf{q}_h(0)\right\|^2+\left\|u_h(0)\right\|^2+(b-a)^{1/2}(d-c)^{1/2}\max_{t\in[0,T]}\left\|u_h(t)\right\|.\end{aligned}$$

Thus, the following inequality holds, $\forall\ t \in [0,T]$,

$$\begin{aligned}&\frac{1}{2}\frac{d^2\left\|u_h\right\|^2}{dt^2}+\frac{\beta}{2}\frac{d\left\|u_h\right\|^2}{dt}\\&\leq\left\|(u_h)_t(0)\right\|^2+\left\|\mathbf{q}_h(0)\right\|^2+\left\|u_h(0)\right\|^2+(b-a)^{1/2}(d-c)^{1/2}\max_{t\in[0,T]}\left\|u_h(t)\right\|.\end{aligned}$$

Integrating in time from 0 to t gives, $\forall\ t \in [0,T]$,

$$\begin{aligned}&\frac{1}{2}\frac{d\left\|u_h\right\|^2}{dt}+\frac{\beta}{2}\left\|u_h\right\|^2\leq\iint_\Omega u_h(x,y,0)(u_h)_t(x,y,0)dxdy+\frac{\beta}{2}\left\|u_h(0)\right\|^2\\&+t\left(\left\|(u_h)_t(0)\right\|^2+\left\|\mathbf{q}_h(0)\right\|^2+\left\|u_h(0)\right\|^2\right)+t(b-a)^{1/2}(d-c)^{1/2}\max_{t\in[0,T]}\left\|u_h(t)\right\|,\end{aligned}$$

which, after applying the Cauchy-Schwarz inequality and the inequality $2ab \leq a^2+b^2$, gives, $\forall\ t \in [0,T]$,

$$\begin{aligned}\frac{d\left\|u_h\right\|^2}{dt}+\beta\left\|u_h\right\|^2\ \leq\ &(1+\beta)\left\|u_h(0)\right\|^2+\left\|(u_h)_t(0)\right\|^2\\&+2t\left(\left\|(u_h)_t(0)\right\|^2+\left\|\mathbf{q}_h(0)\right\|^2+\left\|u_h(0)\right\|^2\right)\\&+2t(b-a)^{1/2}(d-c)^{1/2}\max_{t\in[0,T]}\left\|u_h(t)\right\|.\end{aligned}$$

Since $\beta \geq 0$, the following estimate holds

$$\begin{aligned}\frac{d\left\|u_h\right\|^2}{dt}\ \leq\ &(1+\beta)\left\|u_h(0)\right\|^2+\left\|(u_h)_t(0)\right\|^2\\&+2t\left(\left\|(u_h)_t(0)\right\|^2+\left\|\mathbf{q}_h(0)\right\|^2+\left\|u_h(0)\right\|^2\right)\\&+2t(b-a)^{1/2}(d-c)^{1/2}\max_{t\in[0,T]}\left\|u_h(t)\right\|.\end{aligned}$$

Integrating again in time from 0 to t, we get, $\forall\ t \in [0,T]$,

$$\begin{aligned}\left\|u_h(t)\right\|^2\leq\ &\left\|u_h(0)\right\|^2+t\left((1+\beta)\left\|u_h(0)\right\|^2+\left\|(u_h)_t(0)\right\|^2\right)\\&+t^2\left(\left\|(u_h)_t(0)\right\|^2+\left\|\mathbf{q}_h(0)\right\|^2+\left\|u_h(0)\right\|^2\right)\\&+t^2(b-a)^{1/2}(d-c)^{1/2}\max_{t\in[0,T]}\left\|u_h(t)\right\|.\end{aligned}$$

Using the inequality $ab \leq \frac{1}{2}a^2+\frac{1}{2}b^2$, gives, $\forall\ t \in [0,T]$,

$$\begin{aligned}\left\|u_h(t)\right\|^2\leq\ &\left\|u_h(0)\right\|^2+T\left((1+\beta)\left\|u_h(0)\right\|^2+\left\|(u_h)_t(0)\right\|^2\right)\\&+T^2\left(\left\|(u_h)_t(0)\right\|^2+\left\|\mathbf{q}_h(0)\right\|^2+\left\|u_h(0)\right\|^2\right)\\&+\frac{1}{2}T^4(b-a)(d-c)+\frac{1}{2}\max_{t\in[0,T]}\left\|u_h(t)\right\|^2.\end{aligned}$$

Taking the maximum on both sides with respect to t, we get

$$\begin{aligned}\max_{t\in[0,T]}\left\|u_h(t)\right\|^2\ \leq\ &2\left\|u_h(0)\right\|^2+2T\left((1+\beta)\left\|u_h(0)\right\|^2+\left\|(u_h)_t(0)\right\|^2\right)\\&+2T^2\left(\left\|(u_h)_t(0)\right\|^2+\left\|\mathbf{q}_h(0)\right\|^2+\left\|u_h(0)\right\|^2\right)\\&+T^4(b-a)(d-c),\quad\forall\ t\in[0,T],\end{aligned}$$

which completes the proof of the theorem. □

Remark 3.2. *The estimate (20b) indicates that the upper bound for $\|u_h(t)\|$ grows quadratically in time. We were not able to obtain sharpened bound for $\|u_h(t)\|$. Even in the 1-D linear case, it is well-known that bounds for the LDG errors grow linearly (for convection, convection-diffusion, and wave equations); see e.g.* [32]. *This is also the case for the LDG method applied to the 2-D linear second-order wave equation; see* [33]. *In this paper we proved that $\|u_h(t)\|$ grows quadratically in time. This is due to the nonlinear term involving* $\sin(u_h)$.

From now on, the notation $C,\ C_1,\ C_2,\ C^{\pm}$, etc. will be used to denote positive constants that are independent of the discretization parameters, but which may depend upon the exact smooth solution of the partial differential equation (1a) and its derivatives. Furthermore, all the constants will be generic, *i.e.*, they may represent different constant quantities in different occurrences. Finally, notice that throughout the paper, although $C,\ C_1,\ C_2,\ldots$ do not explicitly depend on t, they are functions of time through the dependence on the norm of u. In this paper, we always assume that the exact solution u is smooth enough. More precisely, we assume that $||u||_{p+3}$ and $||u_t||_{p+2}$ are bounded uniformly for any time $t \in [0,T]$. Consequently, the constants $C,\ C_1,\ C_2,\ldots$ are bounded, namely, for any t, $C,\ C_1,\ C_2,\ldots$ are bounded by a constant C independent of the time t.

4. A priori error estimates for the semi-discrete LDG method

Throughout this paper, e_u and $\mathbf{e_q} = [e_{q,1}, e_{q,2}]^t$ denote the errors between the exact solutions of (3) and the LDG solutions defined in (5) *i.e.*, $e_u = u - u_h$ and $\mathbf{e_q} = \mathbf{q} - \mathbf{q}_h$. Let the projection errors be defined as $\epsilon_u = u - P^- u$ and $\boldsymbol{\epsilon}_\mathbf{q} = \mathbf{q} - \mathbf{P}^+\mathbf{q}$, and the errors between the numerical solutions and the projection of the exact solutions be defined as $\bar{e}_u = P^- u - u_h$ and $\bar{\mathbf{e}}_\mathbf{q} = \mathbf{P}^+\mathbf{q} - \mathbf{q}_h$. We note that the true errors can be split as

$$e_u = \epsilon_u + \bar{e}_u, \quad \mathbf{e_q} = \boldsymbol{\epsilon}_\mathbf{q} + \bar{\mathbf{e}}_\mathbf{q}. \tag{27}$$

In order to prove our optimal error estimates for the LDG scheme, we need to derive the error equations. Subtracting (5a) from (4a) with $v \in V_h^p$ and (5b) from (4b) with $\mathbf{w} \in \mathbf{V}_h^p$, we obtain the following error equations of the LDG scheme on Δ

$$\begin{aligned}
&\iint_\Delta \left((e_u)_{tt} + \beta(e_u)_t + \sin(u) - \sin(u_h)\right) v dxdy \\
&\quad + \iint_\Delta \mathbf{e_q}\cdot\nabla v dxdy - \int_{\Gamma^-} v^+ \mathbf{e}_\mathbf{q}^+ \cdot \mathbf{n} ds - \int_{\Gamma^+} v^- \mathbf{e}_\mathbf{q}^+ \cdot \mathbf{n} ds = 0, \\
&\iint_\Delta \mathbf{e_q}\cdot\mathbf{w} dxdy + \iint_\Delta e_u \nabla\cdot\mathbf{w} dxdy - \int_{\Gamma^-} e_u^- \mathbf{w}^+\cdot\mathbf{n} ds - \int_{\Gamma^+} e_u^- \mathbf{w}^-\cdot\mathbf{n} ds = 0.
\end{aligned}$$

Applying the classical Taylor's series with integral remainder in the variable u and using the relation $u - u_h = e_u$, we write

$$\sin(u) - \sin(u_h) = \theta(u - u_h) = \theta e_u, \tag{29}$$

where $\theta = \theta(x,y,t) = \int_0^1 \cos(u + s(u_h - u))ds = \int_0^1 \cos(u - se_u)ds$.

Using (29), (27), (9), and the property of the projection $\mathbf{P}^+$ given by (12), we rewrite the error equations as

$$\begin{aligned}
&\iint_\Delta \left((e_u)_{tt} + \beta(e_u)_t + \theta e_u\right) v dxdy + \iint_\Delta \bar{\mathbf{e}}_\mathbf{q}\cdot\nabla v dxdy - \int_{\Gamma^-} v^+ \bar{\mathbf{e}}_\mathbf{q}^+ \cdot \mathbf{n} ds \\
&\quad - \int_{\Gamma^+} v^- \bar{\mathbf{e}}_\mathbf{q}^+ \cdot \mathbf{n} ds = 0,
\end{aligned} \tag{30a}$$

(30b)
$$\iint_{\Delta} \mathbf{e_q}\cdot\mathbf{w}dxdy+\iint_{\Delta} \bar{e}_u\nabla\cdot\mathbf{w}dxdy-\int_{\Gamma^-} \bar{e}_u^-\mathbf{w}^+\cdot\mathbf{n}ds-\int_{\Gamma^+} \bar{e}_u^-\mathbf{w}^-\cdot\mathbf{n}ds+Z_{\Delta}(u,\mathbf{w})=0,$$

which, after using a simple integration by parts, are equivalent to

$$\begin{aligned}&\iint_{\Delta}\left((e_u)_{tt}+\beta(e_u)_t+\theta e_u\right)vdxdy-\iint_{\Delta}\nabla\cdot\bar{\mathbf{e}}_{\mathbf{q}}vdxdy\\ &-\int_{\Gamma^+} v^-(\bar{\mathbf{e}}_{\mathbf{q}}^+-\bar{\mathbf{e}}_{\mathbf{q}}^-)\cdot\mathbf{n}ds=0,\end{aligned}\tag{31a}$$

$$\begin{aligned}&\iint_{\Delta}\mathbf{e_q}\cdot\mathbf{w}dxdy-\iint_{\Delta}\nabla\bar{e}_u\cdot\mathbf{w}dxdy\\ &+\int_{\Gamma^-}(\bar{e}_u^+-\bar{e}_u^-)\mathbf{w}^+\cdot\mathbf{n}ds+Z_{\Delta}(u,\mathbf{w})=0.\end{aligned}\tag{31b}$$

We note that

$$\left|\theta\right|\le\int_0^1\left|\cos(u-se_u)\right|ds\le 1,\quad\forall\ (x,y)\in\Omega,\quad\forall\ t\in[0,T].\tag{32}$$

Furthermore, using the smoothness of u_t, we have, $\forall\ (x,y)\in\Omega$ and $\forall\ t\in[0,T]$,

$$\begin{aligned}\left|\theta_t\right| &= \left|-\int_0^1(u_t-s(e_u)_t)\sin(u-se_u)ds\right|\\ &\le \int_0^1\left(\left|u_t\right|+s\left|(e_u)_t\right|\right)\left|\sin(u-se_u)\right|ds\le\int_0^1(C+\left|(e_u)_t\right|)ds=C+\left|(e_u)_t\right|.\end{aligned}\tag{33}$$

Next, we state and prove some preliminary results which will be needed to prove the optimal L^2 error estimates for $\|e_u\|$ and $\|\mathbf{e_q}\|$.

Theorem 4.1. *Let $(u,\mathbf{q})$ be the exact solution of (3) with $u\in H^{p+3}(\Omega)$ and $u_t\in H^{p+2}(\Omega)$. Also, let $(u_h,\mathbf{q}_h)$ be the numerical solution of (5) subject to (14), then there exists a positive constant C depends on $\|u\|_{p+3}$ and $\|u_t\|_{p+2}$ but independent of h such that,*

$$\|\bar{e}_u(0)\|=\|(\bar{e}_u)_t(0)\|=0.\tag{34}$$

$$\|\bar{\mathbf{e}}_{\mathbf{q}}(0)\|\le C\ h^{p+1}.\tag{35}$$

$$\|(\bar{e}_u)_t\|^2\le C(t+1)^2h^{2p+2}+16t\int_0^t\|\bar{e}_u(s)\|^2ds,\quad\forall\ t\in[0,T].\tag{36}$$

$$\|\bar{\mathbf{e}}_{\mathbf{q}}\|\le C(t+1)^2h^{2p+2}+16t\int_0^t\|\bar{e}_u(s)\|^2ds,\quad\forall\ t\in[0,T].\tag{37}$$

Proof. Because of the way the initial conditions (14) are chosen, we have

$$\begin{aligned}\bar{e}_u(x,y,0)=&P^-u(x,y,0)-u_h(x,y,0)=P^-u(x,y,0)-P^-u(x,y,0)=0,\\ (\bar{e}_u)_t(x,y,0)=&P^-u_t(x,y,0)-(u_h)_t(x,y,0)=P^-u_t(x,y,0)-P^-u_t(x,y,0)=0.\end{aligned}$$

Thus, the estimates in (34) hold.

To estimate $\|\bar{\mathbf{e}}_{\mathbf{q}}(0)\|$, we take $t=0$ in the error equation (30b) and use $\bar{e}_u(x,y,0)=0$ to obtain, at $t=0$,

$$\iint_{\Delta}\mathbf{e_q}\cdot\mathbf{w}dxdy+Z_{\Delta}(u,\mathbf{w})=0,\tag{38}$$

which, after taking $\mathbf{w} = \bar{\mathbf{e}}_{\mathbf{q}}(x, y, 0)$, summing over all elements, and using (27), yields

$$\iint_{\Omega} \bar{\mathbf{e}}_{\mathbf{q}} \cdot \bar{\mathbf{e}}_{\mathbf{q}} dxdy = -\iint_{\Omega} \boldsymbol{\epsilon}_{\mathbf{q}} \cdot \bar{\mathbf{e}}_{\mathbf{q}} dxdy - \sum_{\Delta \in \mathcal{T}_h} Z_{\Delta}(u, \bar{\mathbf{e}}_{\mathbf{q}}).$$

Applying Cauchy-Schwarz inequality and using the estimates (10) and (13), we get, at $t = 0$,

$$\begin{aligned} \|\bar{\mathbf{e}}_{\mathbf{q}}(0)\|^2 = \iint_{\Omega} \bar{\mathbf{e}}_{\mathbf{q}} \cdot \bar{\mathbf{e}}_{\mathbf{q}} dxdy &\leq \|\boldsymbol{\epsilon}_{\mathbf{q}}(0)\| \, \|\bar{\mathbf{e}}_{\mathbf{q}}(0)\| + \sum_{\Delta \in \mathcal{T}_h} \left| Z_{\Delta}(u, \bar{\mathbf{e}}_{\mathbf{q}}) \right| \\ &\leq Ch^{p+1} \, \|\bar{\mathbf{e}}_{\mathbf{q}}(0)\| + Ch^{p+1} \, \|u(0)\|_{p+2} \, \|\bar{\mathbf{e}}_{\mathbf{q}}(0)\| . \end{aligned}$$

Consequently, $\|\bar{\mathbf{e}}_{\mathbf{q}}(0)\| = \mathcal{O}(h^{p+1})$, which completes the proof of (35).

Finally, we will prove (36) and (37). Choosing $v = (\bar{e}_u)_t$ in (31a) and taking the first time derivative of (30b) and choosing the test function $\mathbf{w} = \bar{\mathbf{e}}_{\mathbf{q}}$, we obtain

$$\begin{aligned} &\iint_{\Delta} \left((e_u)_{tt} + \beta (e_u)_t + \theta e_u \right) (\bar{e}_u)_t dxdy - \iint_{\Delta} \nabla \cdot \bar{\mathbf{e}}_{\mathbf{q}} (\bar{e}_u)_t dxdy \\ &- \int_{\Gamma^+} (\bar{e}_u)_t^- (\bar{\mathbf{e}}_{\mathbf{q}}^+ - \bar{\mathbf{e}}_{\mathbf{q}}^-) \cdot \mathbf{n} ds = 0, \end{aligned}$$

$$\begin{aligned} &\iint_{\Delta} (\mathbf{e}_{\mathbf{q}})_t \cdot \bar{\mathbf{e}}_{\mathbf{q}} dxdy + \iint_{\Delta} (\bar{e}_u)_t \nabla \cdot \bar{\mathbf{e}}_{\mathbf{q}} dxdy - \int_{\Gamma^-} (\bar{e}_u)_t^- \bar{\mathbf{e}}_{\mathbf{q}}^+ \cdot \mathbf{n} ds \\ &- \int_{\Gamma^+} (\bar{e}_u)_t^- \bar{\mathbf{e}}_{\mathbf{q}}^- \cdot \mathbf{n} ds + Z_{\Delta}(u_t, \bar{\mathbf{e}}_{\mathbf{q}}) = 0. \end{aligned}$$

Adding the above two equations, we get

$$\begin{aligned} &\iint_{\Delta} \left((e_u)_{tt} + \beta (e_u)_t + \theta e_u \right) (\bar{e}_u)_t dxdy + \iint_{\Delta} (\mathbf{e}_{\mathbf{q}})_t \cdot \bar{\mathbf{e}}_{\mathbf{q}} dxdy \\ &- \int_{\Gamma^+} (\bar{e}_u)_t^- \bar{\mathbf{e}}_{\mathbf{q}}^+ \cdot \mathbf{n} ds - \int_{\Gamma^-} (\bar{e}_u)_t^- \bar{\mathbf{e}}_{\mathbf{q}}^+ \cdot \mathbf{n} ds + Z_{\Delta}(u_t, \bar{\mathbf{e}}_{\mathbf{q}}) = 0. \end{aligned}$$

Summing over all elements, applying the periodic or compactly supported boundary conditions, and using (27) yields

$$\begin{aligned} \frac{1}{2} \frac{d}{dt} \left(\|(\bar{e}_u)_t\|^2 + \|\bar{\mathbf{e}}_{\mathbf{q}}\|^2 \right) + \beta \, \|(\bar{e}_u)_t\|^2 = &- \iint_{\Omega} \left(\theta(\epsilon_u + \bar{e}_u) + (\epsilon_u)_{tt} \right) (\bar{e}_u)_t dxdy \\ &- \iint_{\Omega} (\boldsymbol{\epsilon}_{\mathbf{q}})_t \bar{\mathbf{e}}_{\mathbf{q}} dxdy - \sum_{\Delta \in \mathcal{T}_h} Z_{\Delta}(u_t, \bar{\mathbf{e}}_{\mathbf{q}}). \end{aligned}$$

Consequently, we have

$$\begin{aligned} \frac{1}{2} \frac{d}{dt} \left(\|(\bar{e}_u)_t\|^2 + \|\bar{\mathbf{e}}_{\mathbf{q}}\|^2 \right) \leq &\iint_{\Omega} \left(|\theta| (|\epsilon_u| + |\bar{e}_u|) + |(\epsilon_u)_{tt}| \right) |(\bar{e}_u)_t| dxdy \\ &+ \iint_{\Omega} \left| (\boldsymbol{\epsilon}_{\mathbf{q}})_t \right| \left| \bar{\mathbf{e}}_{\mathbf{q}} \right| dxdy + \sum_{\Delta \in \mathcal{T}_h} \left| Z_{\Delta}(u_t, \bar{\mathbf{e}}_{\mathbf{q}}) \right|. \end{aligned} \tag{40}$$

Applying the estimate (32), the Cauchy-Schwarz inequality, the projection result (13), and the estimate (10) leads to

$$\begin{aligned}
&\frac{1}{2}\frac{d}{dt}\left(\|(\bar{e}_u)_t\|^2+\|\bar{\mathbf{e}}_{\mathbf{q}}\|^2\right)\\
\leq\ & \left(\|\epsilon_u\|+\|\bar{e}_u\|+\|(\epsilon_u)_{tt}\|\right)\|(\bar{e}_u)_t\|+\|(\boldsymbol{\epsilon}_{\mathbf{q}})_t\|\,\|\bar{\mathbf{e}}_{\mathbf{q}}\|+Ch^{p+1}\|u_t\|_{p+2}\|\bar{\mathbf{e}}_{\mathbf{q}}\|\\
\leq\ & \left(C_1h^{p+1}+\|\bar{e}_u\|+C_2h^{p+1}\right)\|(\bar{e}_u)_t\|+C_3h^{p+1}\|\bar{\mathbf{e}}_{\mathbf{q}}\|\\
\leq\ & \left(C_4h^{p+1}+\|\bar{e}_u\|\right)\left(\|(\bar{e}_u)_t\|+\|\bar{\mathbf{e}}_{\mathbf{q}}\|\right),
\end{aligned}$$

where $C_4=\max(C_1,C_2,C_3)$.

Applying the inequality $a+b\leq\sqrt{2}(a^2+b^2)^{1/2}$ with $a=\|(\bar{e}_u)_t\|$ and $b=\|\bar{\mathbf{e}}_{\mathbf{q}}\|$, we establish that

$$\frac{1}{2}\frac{d}{dt}\left(\|(\bar{e}_u)_t\|^2+\|\bar{\mathbf{e}}_{\mathbf{q}}\|^2\right)\leq\sqrt{2}(C_4h^{p+1}+\|\bar{e}_u\|)\left(\|(\bar{e}_u)_t\|^2+\|\bar{\mathbf{e}}_{\mathbf{q}}\|^2\right)^{1/2},$$

which leads to

$$\frac{d}{dt}\left(\|(\bar{e}_u)_t\|^2+\|\bar{\mathbf{e}}_{\mathbf{q}}\|^2\right)^{1/2}\leq Ch^{p+1}+2\sqrt{2}\,\|\bar{e}_u\|.$$

Integrating over the interval $[0,t]$, we obtain

$$\left(\|(\bar{e}_u)_t\|^2+\|\bar{e}_q\|^2\right)^{1/2}\leq C\,t\,h^{p+1}+\left(\|(\bar{e}_u)_t(0)\|^2+\|\bar{e}_q(0)\|^2\right)^{1/2}+2\sqrt{2}\int_0^t\|\bar{e}_u(s)\|\,ds.$$

Using the estimates (35), (34), and applying the Cauchy-Schwarz inequality yields

$$\left(\|(\bar{e}_u)_t\|^2+\|\bar{\mathbf{e}}_{\mathbf{q}}\|^2\right)^{1/2}\leq C(t+1)h^{p+1}+2\sqrt{2}t^{1/2}\left(\int_0^t\|\bar{e}_u(s)\|^2\,ds\right)^{1/2},\quad\forall\,t\in[0,T].$$

Squaring both sides and using the inequality $(a+b)^2\leq 2a^2+2b^2$, completes the proof of (36) and (37). □

Now, we are ready to prove several optimal L^2 error estimates for the semi-discrete formulation.

Theorem 4.2. *Under the assumptions of Theorem 4.1, there exists a positive constant C independent of h such that,*

$$\|\bar{e}_u\|\leq Ch^{p+1},\quad\forall\,t\in[0,T]. \tag{41}$$

$$\|(\bar{e}_u)_t\|\leq Ch^{p+1},\quad\forall\,t\in[0,T]. \tag{42}$$

$$\|\bar{\mathbf{e}}_{\mathbf{q}}\|\leq Ch^{p+1},\quad\forall\,t\in[0,T]. \tag{43}$$

$$\|e_u\|\leq Ch^{p+1},\quad\forall\,t\in[0,T]. \tag{44}$$

$$\|(e_u)_t\|\leq Ch^{p+1},\quad\forall\,t\in[0,T]. \tag{45}$$

$$\|\mathbf{e}_{\mathbf{q}}\|\leq Ch^{p+1},\quad\forall\,t\in[0,T]. \tag{46}$$

Proof. In order to prove (41), we choose $v=\bar{e}_u$ in (31a) and $w=\bar{e}_q$ in (30b) to obtain

$$\iint_\Delta\left((e_u)_{tt}+\beta(e_u)_t+\theta e_u\right)\bar{e}_u dxdy-\iint_\Delta\nabla\cdot\bar{\mathbf{e}}_{\mathbf{q}}\bar{e}_u dxdy-\int_{\Gamma^+}\bar{e}_u^-(\bar{\mathbf{e}}_{\mathbf{q}}^+-\bar{\mathbf{e}}_{\mathbf{q}}^-)\cdot\mathbf{n}ds=0, \tag{47}$$

$$\iint_\Delta\mathbf{e}_{\mathbf{q}}\cdot\bar{\mathbf{e}}_{\mathbf{q}}dxdy+\iint_\Delta\bar{e}_u\nabla\cdot\bar{\mathbf{e}}_{\mathbf{q}}dxdy-\int_{\Gamma^-}\bar{e}_u^-\bar{\mathbf{e}}_{\mathbf{q}}^+\cdot\mathbf{n}ds-\int_{\Gamma^+}\bar{e}_u^-\bar{\mathbf{e}}_{\mathbf{q}}^-\cdot\mathbf{n}ds+Z_\Delta(u,\bar{\mathbf{e}}_{\mathbf{q}})=0. \tag{48}$$

Adding (47) to (48), we obtain

$$\begin{aligned}&\iint_{\Delta}\left((e_u)_{tt}+\beta(e_u)_t+\theta e_u\right)\bar{e}_u dxdy+\iint_{\Delta}\mathbf{e_q}\cdot\bar{\mathbf{e}}_{\mathbf{q}}dxdy\\&=\int_{\Gamma^-}\bar{e}_u^-\bar{\mathbf{e}}_{\mathbf{q}}^+\cdot\mathbf{n}ds+\int_{\Gamma^+}\bar{e}_u^-\bar{\mathbf{e}}_{\mathbf{q}}^+\cdot\mathbf{n}ds-Z_{\Delta}(u,\bar{\mathbf{e}}_{\mathbf{q}}).\end{aligned}$$

Summing over all elements yields

$$\begin{aligned}&\iint_{\Omega}\left((e_u)_{tt}+\beta(e_u)_t+\theta e_u\right)\bar{e}_u dxdy+\iint_{\Omega}\mathbf{e_q}\cdot\bar{\mathbf{e}}_{\mathbf{q}}dxdy\\&=\int_{\partial\Omega^-}\bar{e}_u^-\bar{\mathbf{e}}_{\mathbf{q}}^+\cdot\mathbf{n}ds+\int_{\partial\Omega^+}\bar{e}_u^-\bar{\mathbf{e}}_{\mathbf{q}}^+\cdot\mathbf{n}ds-\sum_{\Delta\in\mathcal{T}_h}Z_{\Delta}(u,\bar{\mathbf{e}}_{\mathbf{q}}).\end{aligned}$$

Applying the periodic or compactly supported boundary conditions yields

$$\iint_{\Omega}\left((e_u)_{tt}+\beta(e_u)_t+\theta e_u\right)\bar{e}_u dxdy+\iint_{\Omega}\mathbf{e_q}\cdot\bar{\mathbf{e}}_{\mathbf{q}}dxdy=-\sum_{\Delta\in\mathcal{T}_h}Z_{\Delta}(u,\bar{\mathbf{e}}_{\mathbf{q}}),$$

which, after using (27), is equivalent to

$$\begin{aligned}&\iint_{\Omega}(\bar{e}_u)_{tt}\bar{e}_u dxdy+\beta\iint_{\Omega}(\bar{e}_u)_t\bar{e}_u dxdy+\left\|\bar{\mathbf{e}}_{\mathbf{q}}\right\|^2\\&=-\iint_{\Omega}\left((\epsilon_u)_{tt}+\beta(\epsilon_u)_t+\theta\epsilon_u\right)\bar{e}_u dxdy\\&\quad-\iint_{\Omega}\boldsymbol{\epsilon}_{\mathbf{q}}\cdot\bar{\mathbf{e}}_{\mathbf{q}}dxdy-\sum_{\Delta\in\mathcal{T}_h}Z_{\Delta}(u,\bar{\mathbf{e}}_{\mathbf{q}}).\end{aligned}$$

Using the fact that $(\bar{e}_u)_{tt}\bar{e}_u=(\bar{e}_u(\bar{e}_u)_t)_t-((\bar{e}_u)_t)^2=\frac{1}{2}\left(\bar{e}_u^2\right)_{tt}-((\bar{e}_u)_t)^2$, we obtain

$$\begin{aligned}&\frac{1}{2}\frac{d^2\left\|\bar{e}_u\right\|^2}{dt^2}+\frac{\beta}{2}\frac{d\left\|\bar{e}_u\right\|^2}{dt}+\left\|\bar{\mathbf{e}}_{\mathbf{q}}\right\|^2\\&\qquad=\left\|(\bar{e}_u)_t\right\|^2-\iint_{\Omega}\left((\epsilon_u)_{tt}+\beta(\epsilon_u)_t+\theta\epsilon_u\right)\bar{e}_u dxdy\\&\qquad\quad-\iint_{\Omega}\boldsymbol{\epsilon}_{\mathbf{q}}\cdot\bar{\mathbf{e}}_{\mathbf{q}}dxdy-\sum_{\Delta\in\mathcal{T}_h}Z_{\Delta}(u,\bar{\mathbf{e}}_{\mathbf{q}}).\end{aligned}$$

Using the triangle inequality, the estimate (32), the Cauchy-Schwarz inequality, the projection result (13), and the estimate (10), we get

$$\begin{aligned}&\frac{1}{2}\frac{d^2\left\|\bar{e}_u\right\|^2}{dt^2}+\frac{\beta}{2}\frac{d\left\|\bar{e}_u\right\|^2}{dt}+\left\|\bar{\mathbf{e}}_{\mathbf{q}}\right\|^2\\\leq\;&\left\|(\bar{e}_u)_t\right\|^2+\iint_{\Omega}\left(\left|(\epsilon_u)_{tt}\right|+|\theta|(|\epsilon_u|+|\bar{e}_u|)\right)|\bar{e}_u|dxdy\\&+\iint_{\Omega}\left|\boldsymbol{\epsilon}_{\mathbf{q}}\right|\left|\bar{\mathbf{e}}_{\mathbf{q}}\right|dxdy+\sum_{\Delta\in\mathcal{T}_h}\left|Z_{\Delta}(u,\bar{\mathbf{e}}_{\mathbf{q}})\right|\\\leq\;&\left\|(\bar{e}_u)_t\right\|^2+\left(\left\|(\epsilon_u)_{tt}\right\|+\left\|\epsilon_u\right\|\right)\left\|\bar{e}_u\right\|+\left\|\bar{e}_u\right\|^2+\left\|\boldsymbol{\epsilon}_{\mathbf{q}}\right\|\left\|\bar{\mathbf{e}}_{\mathbf{q}}\right\|+Ch^{p+1}\left\|\bar{\mathbf{e}}_{\mathbf{q}}\right\|\\\leq\;&\left\|(\bar{e}_u)_t\right\|^2+C_1h^{p+1}\left\|\bar{e}_u\right\|+\left\|\bar{e}_u\right\|^2+C_2h^{p+1}\left\|\bar{\mathbf{e}}_{\mathbf{q}}\right\|.\end{aligned}$$

Applying the inequality $ab \le \frac{a^2}{2} + \frac{b^2}{2}$, we obtain

$$\begin{aligned} & \frac{1}{2}\frac{d^2\left\|\bar{e}_u\right\|^2}{dt^2} + \frac{\beta}{2}\frac{d\left\|\bar{e}_u\right\|^2}{dt} + \left\|\bar{\mathbf{e}}_{\mathbf{q}}\right\|^2 \\ \le \quad & \left\|(\bar{e}_u)_t\right\|^2 + \frac{C_1^2}{2}h^{2p+2} + \frac{3}{2}\left\|\bar{e}_u\right\|^2 + \frac{C_2^2}{2}h^{2p+2} + \frac{1}{2}\left\|\bar{\mathbf{e}}_{\mathbf{q}}\right\|^2. \end{aligned}$$

Therefore, the following estimate holds, $\forall\ t \in [0,T]$,

$$\frac{1}{2}\frac{d^2\left\|\bar{e}_u\right\|^2}{dt^2} + \frac{\beta}{2}\frac{d\left\|\bar{e}_u\right\|^2}{dt} \le C_3h^{2p+2} + \frac{3}{2}\left\|\bar{e}_u\right\|^2 + \left\|(\bar{e}_u)_t\right\|^2.$$

Integrating in time from 0 to t, using the estimates (36), and (34) gives

$$\begin{aligned} & \frac{1}{2}\frac{d\left\|\bar{e}_u\right\|^2}{dt} + \frac{\beta}{2}\left\|\bar{e}_u\right\|^2 \le C_3th^{2p+2} + \frac{3}{2}\int_0^t \left\|\bar{e}_u(s)\right\|^2 ds + \int_0^t \left\|(\bar{e}_u)_t(s)\right\|^2 ds \\ \le \quad & C_3th^{2p+2} + \frac{3}{2}\int_0^t \left\|\bar{e}_u(s)\right\|^2 ds \\ & + \frac{C}{3}\left((t+1)^3 - 1\right)h^{2p+2} + 16\int_0^t r\int_0^r \left\|\bar{e}_u(s)\right\|^2 dsdr \\ \le \quad & C_3th^{2p+2} + \frac{3}{2}\int_0^t \left\|\bar{e}_u(s)\right\|^2 ds + C_4(t+1)^3h^{2p+2} + 16t\int_0^t\int_0^r \left\|\bar{e}_u(s)\right\|^2 dsdr \\ \le \quad & C_5(t+1)^3h^{2p+2} + \frac{3}{2}\int_0^t \left\|\bar{e}_u(s)\right\|^2 ds + 16t\int_0^t\int_0^r \left\|\bar{e}_u(s)\right\|^2 dsdr. \end{aligned}$$

Using a simple integration by parts, we conclude that

$$\begin{aligned} \frac{d\left\|\bar{e}_u\right\|^2}{dt} \quad \le \quad & \frac{d\left\|\bar{e}_u\right\|^2}{dt} + \beta\left\|\bar{e}_u\right\|^2 \\ \le \quad & 2C_5(t+1)^3h^{2p+2} + 3\int_0^t \left\|\bar{e}_u(s)\right\|^2 ds + 32t\int_0^t (t-r)\left\|\bar{e}_u(r)\right\|^2 dr \\ \le \quad & 2C_5(t+1)^3h^{2p+2} + 3\int_0^t \left\|\bar{e}_u(s)\right\|^2 ds + 32t^2\int_0^t \left\|\bar{e}_u(r)\right\|^2 dr \\ \le \quad & 2C_5(t+1)^3h^{2p+2} + C_2(t+1)^2\int_0^t \left\|\bar{e}_u(s)\right\|^2 ds, \quad \forall\ t \in [0,T]. \end{aligned}$$

Integrating again in time from 0 to t and using (34), we get

$$\begin{aligned} \left\|\bar{e}_u\right\|^2 \quad \le \quad & \left\|\bar{e}_u(0)\right\|^2 + C_6(t+1)^4h^{2p+2} + C_2\int_0^t \left((r+1)^2\int_0^r \left\|\bar{e}_u(s)\right\|^2 ds\right) dr \\ \le \quad & C_6(t+1)^4h^{2p+2} + C_2(t+1)^2\int_0^t \left(\int_0^r \left\|\bar{e}_u(s)\right\|^2 ds\right) dr \\ \le \quad & C_6(t+1)^4h^{2p+2} + C_2(t+1)^2\int_0^t (t-r)\left\|\bar{e}_u(r)\right\|^2 dr \\ \le \quad & C_6(t+1)^4h^{2p+2} + C_2t(t+1)^2\int_0^t \left\|\bar{e}_u(r)\right\|^2 dr \\ \le \quad & C_6(T+1)^4h^{2p+2} + C_2(T+1)^3\int_0^t \left\|\bar{e}_u(r)\right\|^2 dr, \quad \forall\ t \in [0,T]. \end{aligned}$$

Invoking the classical Gronwall inequality, we get

$$\begin{aligned} \left\|\bar{e}_u\right\|^2 \quad \le \quad & C_6(T+1)^4h^{2p+2}e^{C_2(T+1)^3t} \\ \le \quad & C_6(T+1)^4e^{C_2(T+1)^3T}h^{2p+2} \le Ch^{2p+2}, \quad \forall\ t \in [0,T], \end{aligned}$$

which establishes the estimate (41).

Combining (41) with the estimates (36)-(37) yield (42) and (43). Finally, using (27) and applying the triangle inequality and the projection result (13), we establish the estimates (44), (45), and (46). Thus, we have completed the proof of the theorem. □

Remark 4.1. *Our results are valid for arbitrary regular meshes and for $\mathcal{Q}^p$ polynomials and for (i) periodic, (ii) purely Dirichlet, (iii) purely Neumann, and (iv) mixed Dirichlet-Neumann boundary conditions. In our proofs, we consider the case of periodic or compactly supported boundary conditions only to get an energy-conserving scheme.*

Remark 4.2. *The theoretical results of this section hold true for the LDG method applied to more general wave equations of the form*

$$u_{tt} = \Delta u + f(\mathbf{x}, t, u), \quad \mathbf{x} \in \Omega \in \mathbb{R}^d, \ t \in [0, T], \quad d = 1, 2, 3, \tag{49}$$

subject to some appropriate initial and boundary conditions. The error analysis follows in a similar manner if we assume that the nonlinear term $f(\mathbf{x}, t, u)$ satisfies a Lipschitz condition on the set $D = \Omega \times [0, T] \times \mathbb{R}$ in the variable u with uniform Lipschitz constant L, i.e., there exists a constant $L > 0$ with

$$\big|f(\mathbf{x}, t, u) - f(\mathbf{x}, t, v)\big| \leq L\big|u - v\big|, \quad \textit{for all } (\mathbf{x}, t, u) \textit{ and } (\mathbf{x}, t, v) \in D.$$

We note that the sine-Gordon equation is a special case of (49).

5. Numerical examples

In this section, we provide several numerical examples to validate our theoretical results. We will demonstrate the $(p+1)$-th order for the errors of u and $\mathbf{q}$. For simplicity, we use uniform Cartesian meshes obtained by partitioning the computational domain $\Omega = [a, b]^2$ into $N = n \times n$ square elements. All examples are performed using the spaces $\mathcal{Q}^p$. The initial conditions are determined by (14). Time discretization is by the fourth-order explicit Runge-Kutta method with a sufficiently small time step so that error in time is negligible compared to spatial errors. The integrals in the semi-discrete LDG method are evaluated using Gauss-Legendre quadrature. Finally, in all numerical experiments, the rate of convergence is computed by $-\frac{\ln(||e_u^{n_1}||/||e_u^{n_2}||)}{\ln(n_1/n_2)}$, where $e_u^{n_1}$ and $e_u^{n_2}$ denote the errors using $N_1 = n_1^2$ and $N_2 = n_2^2$ elements, respectively.

Example 5.1. In this example, we consider the following inhomogeneous sine-Gordon equation

$$\begin{cases} u_{tt} + \sin(u) = \Delta u + f(x, y, t), \quad (x, y) \in \Omega = [0, 2\pi]^2, \ t \in [0, T], \\ u(x, y, 0) = \sin(x + y), \quad u_t(x, y, 0) = \cos(x + y), \quad (x, y) \in \Omega, \end{cases} \tag{50}$$

subject to the periodic boundary conditions. We select f such that the exact solution is

$$u(x, y, t) = \sin(x + y + t).$$

We solve this problem on a uniform Cartesian mesh having $N = 25$, 100, 400, 900, 1600, and 2500 elements obtained by dividing the computational domain Ω into n^2 square elements with $n = 5$, 10, 20, 30, 40, and 50. We use the spaces $\mathcal{Q}^p$, $p = 0, 1, 2, 3, 4$. In order to demonstrate the $(p+1)$-th order for the errors of u and $\mathbf{q}$, we use the semi-discrete LDG scheme with a sufficiently small time step so that error in time is negligible compared to spatial errors. More precisely, we take $\Delta t = 0.001h^2$, where $h = 2\pi/n$, to reduce the time error. In Figure 1 we show the

actual errors $||e_u||$ and $||\mathbf{e_q}||$ versus n at time $t = 1$. For each $\mathcal{Q}^p$ space, we fit, in a least-squares sense, the data sets with a linear function and then calculate from the fitting result the slopes of the fitting lines. The slopes of the fitting lines are shown on the graph. We observe the $(p + 1)$-th order of accuracy with the spaces $\mathcal{Q}^p$, $p = 0, 1, 2, 3, 4$. Thus, the error estimates proved in this paper are optimal in the exponent of the parameter h. This is in full agreement with the theory.

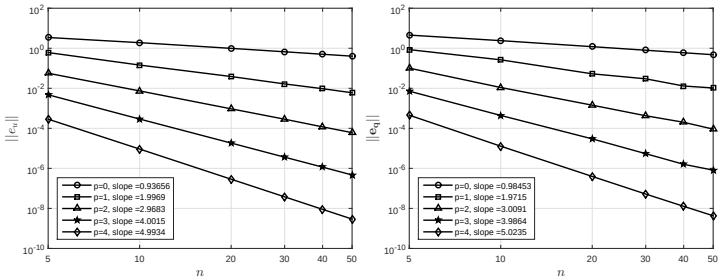

Figure 1: Convergence rates at $t = 1$ for $||e_u||$ (left) and $||\mathbf{e_q}||$ (right) for Example 5.1 on uniform meshes having $N = 25,\ 100,\ 400,\ 900,\ 1600,\ 2500$ square elements using $\mathcal{Q}^p$, $p = 0 - 4$.

Example 5.2. In this example, we consider the homogeneous sine-Gordon equation

$$u_{tt} + \sin(u) = \Delta u, \quad (x, y) \in \Omega = [0, 1]^2,\ t \in [0, 1] \tag{51a}$$

subject to the initial conditions

$$u(x, y, 0) = g(x, y), \quad u_t(x, y, 0) = h(x, y), \quad (x, y) \in \Omega, \tag{51b}$$

and to the mixed Dirichlet-Neumann boundary conditions

(51c)

$$u = g_D, \quad (x, y) \in \partial\Omega_D = \partial\Omega_1^- \cup \partial\Omega_2^-, \quad \frac{\partial u}{\partial n} = \mathbf{g}_N \cdot \mathbf{n}, \quad (x, y) \in \partial\Omega_N = \partial\Omega_1^+ \cup \partial\Omega_2^+,$$

where $\partial\Omega_1^-$, $\partial\Omega_1^+$, $\partial\Omega_2^-$, and $\partial\Omega_2^+$ denote the left, right, bottom, and top edges of the domain $\Omega = [0, 1]^2$, respectively. The initial and boundary conditions are extracted from the exact solution

$$u(x, y, t) = 4 \tan^{-1} (\exp (x + y - t)) .$$

We solve (51) using the same parameters and meshes as in Example 5.1. In Figure 2, we present the L^2-norm of the errors $||e_u||$ and $||\mathbf{e_q}||$ at the final time $t = 1$ as well as their orders of convergence. Again, these results indicate that the convergence order for $||e_u||$ and $||\mathbf{e_q}||$ is $p + 1$, which is in full agreement with the theory.

Example 5.3. In this example, we consider the following problem subject to the purely Dirichlet boundary conditions

$$\begin{cases} u_{tt} + \sin(u) = \Delta u + f(x, y, t), \quad (x, y) \in \Omega = [0, 2\pi]^2,\ t \in [0, 1], \\ u(x, y, 0) = \sin (x + y) , \quad u_t(x, y, 0) = \cos (x + y) , \quad (x, y) \in \Omega, \\ u(0, y, t) = \sin (y + t) , \quad u(2\pi, y, t) = \sin (y + t) , \\ u(x, 0, t) = \sin (x + t) , \quad u(x, 2\pi, t) = \sin (x + t) . \end{cases} \tag{52}$$

We select f such that the exact solution is $u(x, y, t) = \sin (x + y + t)$. We solve (52) using the same parameters and meshes as in Example 5.1. In Figure 3, we present the L^2-norm of the errors $||e_u||$ and $||\mathbf{e_q}||$ at the final time $t = 1$ as well as

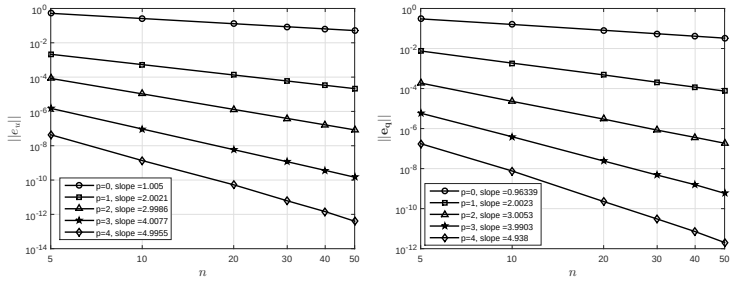

Figure 2: Convergence rates at $t = 1$ for $||e_u||$ (left) and $||\mathbf{e_q}||$ (right) for Example 5.2 on uniform meshes having $N = 25,\ 100,\ 400,\ 900,\ 1600,\ 2500$ square elements using $\mathcal{Q}^p$, $p = 0 - 4$.

their orders of convergence. These results indicate that the convergence order for $||e_u||$ and $||\mathbf{e_q}||$ is $p + 1$. This is in full agreement with the theory.

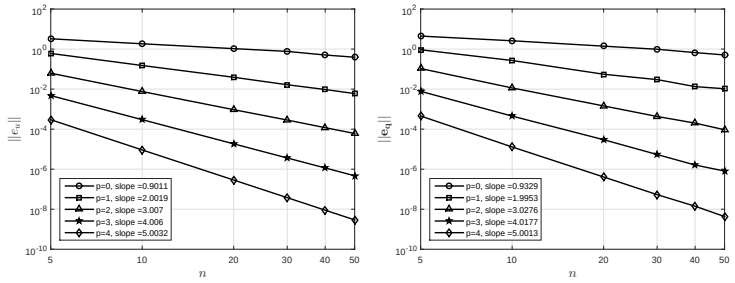

Figure 3: Convergence rates at $t = 1$ for $||e_u||$ (left) and $||\mathbf{e_q}||$ (right) for Example 5.3 on uniform meshes having $N = 25,\ 100,\ 400,\ 900,\ 1600,\ 2500$ square elements using $\mathcal{Q}^p$, $p = 0 - 4$.

Example 5.4 (Superposition of two orthogonal line solitons)**.** In this example, we simulate the superposition of two orthogonal line solitons by considering the sine-Gordon equation in the region $-10 \leq x, y \leq 10$

$$
\begin{cases}
u_{tt} + \sin(u) = \triangle u, \quad (x,y) \in [-10,10]^2,\ t \in [0,T], \\
u(x,y,0) = 4\arctan(\exp(x)) + 4\arctan(\exp(y)), \quad (x,y) \in [-10,10]^2 \\
u_t(x,y,0) = 0, \quad (x,y) \in [-10,10]^2, \\
\frac{\partial u}{\partial n} = 0, \quad (x,y) \in \partial\Omega.
\end{cases} \tag{53}
$$

This test problem was considered in many papers *e.g.*, [5, 28, 34]. The LDG solutions using $p = 1$ and $N = 1600$ are presented in Figure 4 at times $t = 0$, 1, 2, 3, 4, 5, 6, 7, and 10. It can be seen from the graphs that the break up of these two orthogonal line solitons, which are parallel to the diagonal $y = -x$ and are moving away from each other in the direction of $y = x$, is found. These results are in full agreement with those published in [5, 28, 34].

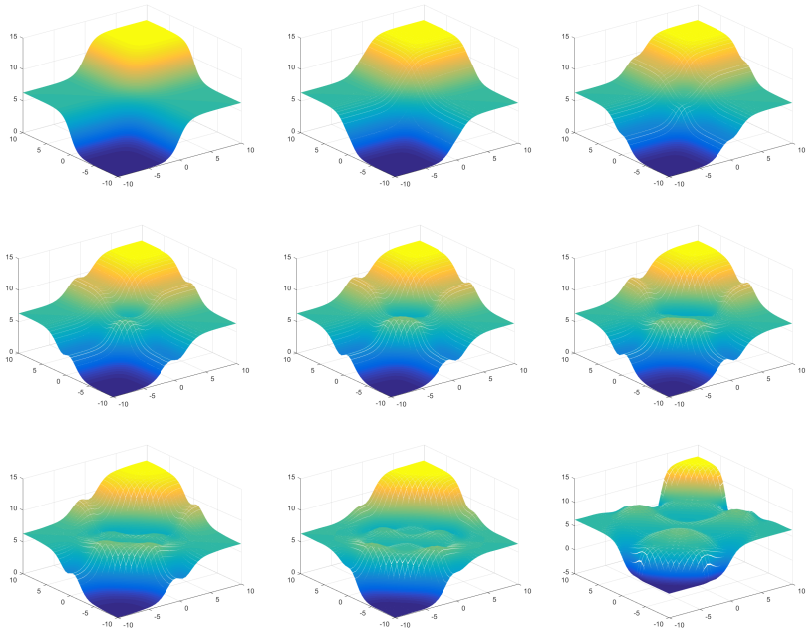

Figure 4: The LDG solutions u_h at $t = 0, 1, 2, 3, 4, 5, 6, 7, 10$ (upper left to lower right) for Example 5.4 using $N = 1600$ and $p = 1$.

The initial energy $E(0)$ is obtained analytically as following

$$\begin{aligned} E(0) =& \frac{1}{2}\int_{-10}^{10}\int_{-10}^{10} \big(u_t^2(x,y,0) \\ &+u_x^2(x,y,0) + u_y^2(x,y,0) + 2(1-\cos(u(x,y,0)))\big)\, dxdy \\ \approx& 303.9999988127755, \end{aligned}$$

where we used Gaussian quadrature to approximate the integral. The results shown in Figures 5-6 suggest that the energy $E_h(t)$ remains approximately as a constant. Thus, our LDG scheme conserves the energy even for large time T. This is in full agreement with the theory. Numerical results further indicate that the energy $E_h(t)$ converges to the initial error with decreasing mesh size.

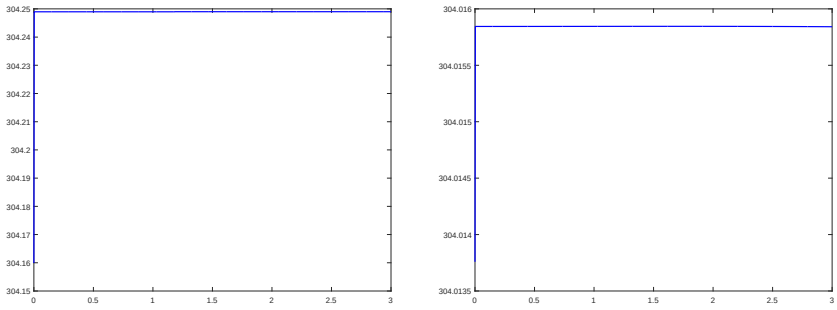

Figure 5: The discrete energy for $t \in [0, 3]$ for Example 5.4 using $(N, p) = (400, 1)$ (left) and $(N, p) = (1600, 1)$ (right).

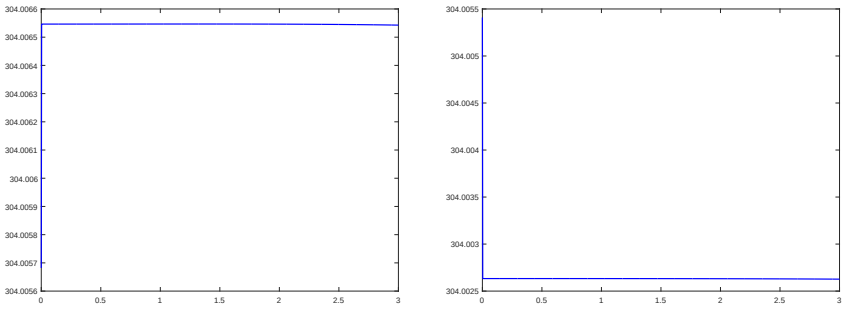

Figure 6: The discrete energy for $t \in [0, 3]$ for Example 5.4 using $(N, p) = (2500, 1)$ (left) and $(N, p) = (400, 2)$ (right).

Remark 5.1. *We would like to emphasize that the energy conservation property is important in order to preserve the phase and shape of the waves. It is well-known that energy-conserving numerical methods (conserve the discrete approximation of the energy) are more suitable for solving wave propagation problems because they are able to maintain the phase and shape of the waves accurately, especially for long time simulation. We simulate the above problems using the same parameters and meshes except the final time* $T = 100$. *We observed that the* L^2 *errors do not grow in time. We also observed that the shape of the solution after long time integration is well preserved. Consult* [4] *and the references cited therein for a detailed discussion of the dispersive and dissipative behaviour of high order DG finite element methods.*

6. Conclusion

In this paper, we proposed and analyzed a high order and energy-conserving LDG method for solving the two-dimensional sine-Gordon nonlinear hyperbolic equation on Cartesian grids. We proved the energy-conserving property, the L^2 stability, and optimal L^2 error estimates for the semi-discrete LDG scheme. More precisely, we identified suitable numerical fluxes and a suitable projection of the initial conditions for the LDG scheme for which the L^2-norm of the solution and its gradient are both of order $p + 1$, when tensor product polynomials of degree at most p are used. Our numerical experiments demonstrate that the proposed scheme yields optimal rates of convergence. The extension of these proofs for 3-D problems on Cartesian meshes is straight forward. We are currently studying the superconvergence properties of the LDG method applied to two-dimensional problems on Cartesian meshes. We are also planning to construct *a posteriori* errors estimates based on superconvergence to construct efficient adaptive high order LDG method for the sine-Gordon equations. Extending the error analysis to problems on triangular and tetrahedral meshes involve many technical difficulties and will be investigated in the future.

References

[1] M. Ablowitz, B. Herbst, and C. Schober. On the numerical solution of the sine-Gordon equation: I. Integrable discretizations and homoclinic manifolds. Journal of Computational Physics, 126(2):299–314, 1996.

[2] M. Ablowitz, B. Herbst, and C. Schober. On the numerical solution of the sine-Gordon equation. Journal of Computational Physics, 131(2):354–367, 1997.

[3] S. Adjerid and M. Baccouch. A superconvergent local discontinuous Galerkin method for elliptic problems. Journal of Scientific Computing, 52:113–152, 2012.

[4] M. Ainsworth, P. Monk, and W. Muniz. Dispersive and dissipative properties of discontinuous Galerkin finite element methods for the second-order wave equation. Journal of Scientific Computing, 27:5–40, 2006.
[5] J. Argyris, M. Haase, and J. C. Heinrich. Finite element approximation to two-dimensional sine-Gordon solitons. Computer Methods in Applied Mechanics and Engineering, 86(1):1 – 26, 1991.
[6] M. Baccouch. A local discontinuous Galerkin method for the second-order wave equation. Computer Methods in Applied Mechanics and Engineering, 209–212:129–143, 2012.
[7] M. Baccouch. Asymptotically exact pha posteriori LDG error estimates for one-dimensional transient convection-diffusion problems. Applied Mathematics and Computation, 226:455 – 483, 2014.
[8] M. Baccouch. The local discontinuous Galerkin method for the fourth-order Euler-Bernoulli partial differential equation in one space dimension. Part I: Superconvergence error analysis. Journal of Scientific Computing, 59:795–840, 2014.
[9] M. Baccouch. The local discontinuous Galerkin method for the fourth-order Euler-Bernoulli partial differential equation in one space dimension. Part II: *A posteriori* error estimation. Journal of Scientific Computing, 60:1–34, 2014.
[10] M. Baccouch. Superconvergence and pha posteriori error estimates for the LDG method for convection-diffusion problems in one space dimension. Computers & Mathematics with Applications, 67:1130–1153, 2014.
[11] M. Baccouch. Superconvergence and pha posteriori error estimates of a local discontinuous Galerkin method for the fourth-order initial-boundary value problems arising in beam theory. International journal of numerical analysis and modeling, series B, 5:188–216, 2014.
[12] M. Baccouch. Superconvergence of the local discontinuous Galerkin method applied to the one-dimensional second-order wave equation. Numerical methods for partial differential equations, 30:862–901, 2014.
[13] M. Baccouch. A superconvergent local discontinuous Galerkin method for the second-order wave equation on cartesian grids. Computers and Mathematics with Applications, 68:1250–1278, 2014.
[14] M. Baccouch. Asymptotically exact *a posteriori* local discontinuous Galerkin error estimates for the one-dimensional second-order wave equation. Numerical methods for partial differential equations, 31:1461–1491, 2015.
[15] M. Baccouch. Asymptotically exact local discontinuous Galerkin error estimates for the linearized Korteweg-de Vries equation in one space dimension. International Journal of Numerical Analysis and Modeling, 12:162–195, 2015.
[16] M. Baccouch. Optimal a posteriori error estimates of the local discontinuous Galerkin method for convection-diffusion problems in one space dimension. Journal of Computational Mathematics, 34:511–531, 2016.
[17] M. Baccouch. An optimal pha posteriori error estimates of the local discontinuous Galerkin method for the second-order wave equation in one space dimension. International Journal of Numerical Analysis and Modeling, 14:355–380, 2017.
[18] M. Baccouch. Optimal energy-conserving local discontinuous Galerkin method for the one-dimensional sine-Gordon equation. International Journal of Computer Mathematics, 94:316–344, 2017.
[19] M. Baccouch. Superconvergence of the local discontinuous Galerkin method for the sine-Gordon equation on cartesian grids. Applied Numerical Mathematics, 113:124 – 155, 2017.
[20] M. Baccouch. A superconvergent local discontinuous Galerkin method for nonlinear two-point boundary-value problems. Numerical Algorithms, Dec 2017. , doi=10.1007/s11075-017-0456-0.
[21] M. Baccouch. A posteriori local discontinuous Galerkin error estimates for the one-dimensional sine-Gordon equation. International Journal of Computer Mathematics, 95(4):815–844, 2018.
[22] M. Baccouch. Superconvergence of the local discontinuous Galerkin method for the sine-Gordon equation in one space dimension. Journal of Computational and Applied Mathematics, 333:292 – 313, 2018.
[23] M. Baccouch. Superconvergence of the semi-discrete local discontinuous Galerkin method for nonlinear KdV-type problems. Discrete and Continuous Dynamical System - B, 24(1)19–54, 2019.

[24] M. Baccouch and S. Adjerid. *A posteriori* local discontinuous Galerkin error estimation for two-dimensional convection-diffusion problems. Journal of Scientific Computing, 62:399–430, 2014.
[25] A. Barone, F. Esposito, C. Magee, and A. Scott. Theory and applications of the sine-Gordon equation. La Rivista del Nuovo Cimento, 1(2):227–267, 1971.
[26] B. Batiha, M. Noorani, and I. Hashim. Numerical solution of sine-Gordon equation by variational iteration method. Physics Letters, Section A: General, Atomic and Solid State Physics, 370(5-6):437–440, 2007.
[27] G. Ben-Yu, P. Pascual, M. Rodriguez, and L. Vzquez. Numerical solution of the sine-Gordon equation. Applied Mathematics and Computation, 18(1):1–14, 1986.
[28] A. Bratsos. The solution of the two-dimensional sine-Gordon equation using the method of lines. Journal of Computational and Applied Mathematics, 206(1):251 – 277, 2007.
[29] A. Bratsos and E. Twizell. A family of parametric finite-difference methods for the solution of the sine-Gordon equation. Applied Mathematics and Computation, 93(2-3):117–137, 1998.
[30] P. Castillo, B. Cockburn, D. Schötzau, and C. Schwab. Optimal a priori error estimates for the *hp*-version of the local discontinuous Galerkin method for convection-diffusion problems. Mathematic of Computation, 71:455–478, 2002.
[31] F. Celiker and B. Cockburn. Superconvergence of the numerical traces for discontinuous Galerkin and hybridized methods for convection-diffusion problems in one space dimension. Mathematics of Computation, 76:67–96, 2007.
[32] Y. Cheng and C.-W. Shu. Superconvergence of discontinuous Galerkin and local discontinuous Galerkin schemes for linear hyperbolic and convection-diffusion equations in one space dimension. SIAM Journal on Numerical Analysis, 47:4044–4072, 2010.
[33] C.-S. Chou, C.-W. Shu, and Y. Xing. Optimal energy conserving local discontinuous Galerkin methods for second-order wave equation in heterogeneous media. Journal of Computational Physics, 272:88–107, 2014.
[34] P. L. Christiansen and P. S. Lomdahl. Numerical study of 2+1 dimensional sine-Gordon solitons. Physica D: Nonlinear Phenomena, 2(3):482 – 494, 1981.
[35] L. Cisneros, J. Ize, and A. Minzoni. Modulational and numerical solutions for the steady discrete sine-Gordon equation in two space dimensions. Physica D: Nonlinear Phenomena, 238(14):1229–1240, 2009.
[36] B. Cockburn, G. Kanschat, I. Perugia, and D. Schötzau. Superconvergence of the local discontinuous Galerkin method for elliptic problems on cartesian grids. SIAM Journal on Numerical Analysis, 39:264–285, 2001.
[37] B. Cockburn, G. E. Karniadakis, and C. W. Shu. Discontinuous Galerkin Methods Theory, Computation and Applications, Lecture Notes in Computational Science and Engineering, volume 11. Springer, Berlin, 2000.
[38] B. Cockburn and C. W. Shu. The local discontinuous Galerkin method for time-dependent convection-diffusion systems. SIAM Journal on Numerical Analysis, 35:2440–2463, 1998.
[39] M. Darvishi, F. Khani, S. Hamedi-Nezhad, and S.-W. Ryu. New modification of the HPM for numerical solutions of the sine-Gordon and coupled sine-Gordon equations. International Journal of Computer Mathematics, 87(4):908–919, 2010.
[40] M. Dehghan and A. Shokri. A numerical method for solution of the two-dimensional sine-Gordon equation using the radial basis functions. Mathematics and Computers in Simulation, 79(3):700–715, 2008.
[41] M. Dehghan and A. Shokri. Numerical solution of the nonlinear Klein-Gordon equation using radial basis functions. Journal of Computational and Applied Mathematics, 230(2):400 – 410, 2009.
[42] K. Djidjeli, W. Price, and E. Twizell. Numerical solutions of a damped sine-Gordon equation in two space variables. Journal of Engineering Mathematics, 29(4):347–369, 1996. cited By 38.
[43] R. K. Dodd. Solitons and nonlinear wave equations. Academic Press, London New York, 1982.
[44] R. K. Dodd, J. C. Eilbeck, J. D. Gibbon, and H. C. Morris. Solitons and nonlinear wave equations. Academic Press, London New York, 1982.
[45] B. Dong and C.-W. Shu. Analysis of a local discontinuous Galerkin method for linear time-dependent fourth-order problems. SIAM Journal on Numerical Analysis, 47:3240–3268, 2009.
[46] R. Flesch, M. Forest, and A. Sinha. Numerical inverse spectral transform for the periodic sine-Gordon equation: Theta function solutions and their linearized stability. Physica D: Nonlinear Phenomena, 48(1):169–231, 1991.

[47] A. Hussain, S. Haq, and M. Uddin. Numerical solution of Klein-Gordon and sine-Gordon equations by meshless method of lines. Engineering Analysis with Boundary Elements, 37(11):1351–1366, 2013.

[48] Z.-W. Jiang and R.-H. Wang. Numerical solution of one-dimensional sine-Gordon equation using high accuracy multiquadric quasi-interpolation. Applied Mathematics and Computation, 218(15):7711–7716, 2012. cited By 7.

[49] S. Jimnez and L. Vzquez. Analysis of four numerical schemes for a nonlinear Klein-Gordon equation. Applied Mathematics and Computation, 35(1):61 – 94, 1990.

[50] D. Kaya. A numerical solution of the sine-Gordon equation using the modified decomposition method. Applied Mathematics and Computation, 143(2-3):309–317, 2003.

[51] G. Kazacha and S. Serdyukov. Numerical investigation of the behaviour of solutions of the sine-Gordon equation with a singularity for large t. Computational Mathematics and Mathematical Physics, 33(3):377–385, 1993.

[52] Y. Keskin, I. Caglar, and A. Koc. Numerical solution of sine-Gordon equation by reduced differential transform method. volume 1, pages 109–113, 2011.

[53] G. L. Lamb. Elements of soliton theory. Wiley, New York, 1980.

[54] P. LeSaint and P. A. Raviart. On a finite element method for solving the neutron transport equations. In C. de Boor, editor, Mathematical Aspects of Finite Elements in Partial Differential Equations, pages 89–123, New York, 1974. Academic Press.

[55] O. Levring, M. Samuelsen, and O. Olsen. Exact and numerical solutions to the perturbed sine-Gordon equation. Physica D: Nonlinear Phenomena, 11(3):349–358, 1984.

[56] X. Meng, C.-W. Shu, and B. Wu. Superconvergence of the local discontinuous Galerkin method for linear fourth-order time-dependent problems in one space dimension. IMA Journal of Numerical Analysis, 32:1294–1328, 2012.

[57] J. Perring and T. Skyrme. A model unified field equation. Nuclear Physics, 31:550 – 555, 1962.

[58] S. Popov. Numerical analysis of soliton solutions of the modified Korteweg-de Vries-sine-Gordon equation. Computational Mathematics and Mathematical Physics, 55(3):437–446, 2015.

[59] S. Ray. A numerical solution of the coupled sine-Gordon equation using the modified decomposition method. Applied Mathematics and Computation, 175(2):1046–1054, 2006.

[60] W. H. Reed and T. R. Hill. Triangular mesh methods for the neutron transport equation. Technical Report LA-UR-73-479, Los Alamos Scientific Laboratory, Los Alamos, 1973.

[61] A. Scott. Active and nonlinear wave propagation in electronics. Wiley-Interscience, New York, 1970.

[62] A. C. Scott. A nonlinear Klein-Gordon equation. American Journal of Physics, 37:52 – 61, 1969.

[63] W. Shao and X. Wu. The numerical solution of the nonlinear Klein-Gordon and sine-Gordon equations using the Chebyshev tau meshless method. Computer Physics Communications, 185(5):1399–1409, 2014.

[64] Q. Sheng, A. M. Khaliq, and D. Voss. Numerical simulation of two-dimensional sine-Gordon solitons via a split cosine scheme. Mathematics and Computers in Simulation, 68(4):355 – 373, 2005.

[65] C.-W. Shu. Discontinuous Galerkin method for time-dependent problems: Survey and recent developments. In X. Feng, O. Karakashian, and Y. Xing, editors, Recent Developments in Discontinuous Galerkin Finite Element Methods for Partial Differential Equations, volume 157 of The IMA Volumes in Mathematics and its Applications, pages 25–62. Springer International Publishing, 2014.

[66] W. Strauss and L. Vazquez. Numerical solution of a nonlinear Klein-Gordon equation. Journal of Computational Physics, 28(2):271 – 278, 1978.

[67] A. Taleei and M. Dehghan. A pseudo-spectral method that uses an overlapping multidomain technique for the numerical solution of sine-Gordon equation in one and two spatial dimensions. Mathematical Methods in the Applied Sciences, 37(13):1909–1923, 2014.

[68] Q.-F. Wang. Numerical solution for series sine-Gordon equations using variational method and finite element approximation. Applied Mathematics and Computation, 168(1):567–599, 2005.

[69] Y. Xu and C.-W. Shu. Local discontinuous Galerkin methods for high-order time-dependent partial differential equations. Communications in Computational Physics, 7:1–46, 2010.

[70] Y. Xu and C.-W. Shu. Optimal error estimates of the semi-discrete local discontinuous Galerkin methods for high order wave equations. SIAM Journal on Numerical Analysis, 50:79–104, 2012.
[71] C. Zheng. Numerical solution to the sine-Gordon equation defined on the whole real axis. SIAM Journal on Scientific Computing, 29(6):2494–2506, 2007.

Department of Mathematics, University of Nebraska at Omaha, Omaha, NE 68182, USA
E-mail: mbaccouch@unomaha.edu